

OPTIMIZATION OF AN ATMOSPHERIC WATER GENERATION SYSTEM USING
PELTIER DEVICES AND MULTIPLE HEAT TRANSFER MECHANISMS

by

Mark Thomas Summers, BSME, MST

A thesis submitted to the Graduate Council of
Texas State University in partial fulfillment
of the requirements for the degree of
Master of Science
with a Major in Engineering
December 2021

Committee Members:

Bahram Asiabanpour, Chair

Namwon Kim

Harold Stern

COPYRIGHT

by

Mark Thomas Summers

2021

FAIR USE AND AUTHOR'S PERMISSION STATEMENT

Fair Use

This work is protected by the Copyright Laws of the United States (Public Law 94-553, section 107). Consistent with fair use as defined in the Copyright Laws, brief quotations from this material are allowed with proper acknowledgement. Use of this material for financial gain without the author's express written permission is not allowed.

Duplication Permission

As the copyright holder of this work I, Mark Thomas Summers, refuse permission to copy in excess of the "Fair Use" exemption without my written permission.

DEDICATION

To Paul Thomas, for inspiring my dad to have an inquiring mind and passion for knowledge, to Kenneth Paul, for instilling in me a balanced approach for family, career, and personally enriching activities, to Jeffrey Paul for teaching me the dedication required and benefits of pursuing your dreams, and to Ronan Michael for giving me confidence for the future of humanity.

ACKNOWLEDGEMENTS

Many thanks to Dr. Bahram Asiabanpour for his guidance during my first attempts at the world of research and to Dr. Vishu Viswanathan for his patience with me during my six-year odyssey to complete my dream of completing an engineering master's degree.

Additional thanks to these professors that were a part of my classroom curriculum.

Dr. Semih Aslan

Dr. Bahram Asiabanpour

Dr. Fred Chen

Dr. Jitendra Tate

Dr. Namwon Kim

Dr. Fred Aguayo

Dr. Vedaraman Sriraman

Dr. Ravi Droopad

TABLE OF CONTENTS

	Page
ACKNOWLEDGEMENTS.....	v
LIST OF TABLES.....	vii
LIST OF FIGURES.....	viii
ABSTRACT.....	x
CHAPTER	
I. INTRODUCTION.....	1
II. DETERMINATION OF AMBIENT CONDITIONS.....	3
III. CASE STUDY – SMART AWG.....	13
IV. IMPROVING HEAT TRANSFER IN AWG.....	21
V. AWG DESIGN PARAMETERS.....	30
VI. AWG SYSTEM DESIGN.....	36
VII. COMPUTATIONAL FLUID DYNAMICS SIMULATION.....	41
VIII. CONCLUSIONS.....	49
IX. SUMMARY AND FUTURE WORK.....	55
REFERENCES.....	57

LIST OF TABLES

Table	Page
1. Psychrometric Chart Parameters.....	5
2. Water From Air Resource (WFAR) Values.....	7
3. Enthalpy Values.....	9
4. RONAN Index Value Grades	10
5. Sample Initial Conditions and Resulting RONAN and WFAR Indices	10
6. Heat Pipe Assembly Dimensions.....	39
7. TEC Supplied Current.....	47
8. Volumetric Airflow Rates.....	50

LIST OF FIGURES

Figure	Page
1. ASHRAE Simplified Sea Level Psychrometric Chart.....	4
2. Ratio of Needed Enthalpy and Net Enthalpy.....	8
3. Constant RONAN Value Family of Curves.....	11
4. Range of RONAN Values at Various Ambient Conditions.....	12
5. Peltier Device.....	15
6. Peltier Device Module	15
7. Arduino Mega Microcontroller.....	16
8. Timed Cycle vs. Smart Sensing.....	18
9. Operating Condition Ratios	19
10. TEC Operational Illustration.....	23
11. Original Four TEC Platform	25
12. Original (12) TEC Platform Isometric View	26
13. Updated Test Platform Exploded View	27
14. Hybrid Heat Sink / Heat Pipe Cooling Assembly.....	27
15. Computation Fluid Dynamics (CFD) Simulation of Four-Way Duct Design	28
16. TEC1-12706 Thermoelectric Cooler	32
17. TEC Component Illustration.....	32
18. TEC Coefficient of Performance Curves.....	33
19. Heat Pipe Component Illustration.....	35

20. Final AWG Test Platform.....	37
21. TEC Grid Configurations.....	38
22. Cooling Air Duct Design Methodology.....	39
23. Heat Sink Assembly Configurations.....	40
24. Heat Sink Assembly Isometric Views	40
25. Mesh Refinement Options	42
26. Navier-Stokes Equations.....	42
27. Fan Curves	44
28. Duct Air Flow Particle Trajectories.....	45
29. Duct Airflow with Heat Sink Assemblies.....	46
30. Condensation Plate Temperature Distribution Profiles	47
31. Condensation Plate Temperature Distribution Profiles	48
32. Comair-Rotron Fan Performance Curve.....	50
33. Condensation Plate Temperature Distribution.....	52
34. Radial Aluminum Finned Heat Sink (www.heatsinkusa.com).....	53
35. Heat Pipe Design Parameters (www.heatsinkusa.com).....	54
36. 127 vs. 199 couple TEC Comparisons: Equal Power	55
37. Heat Pipe Design Parameters.....	56

ABSTRACT

Atmospheric Water Generation (AWG) is the process of extracting liquid water from humid ambient air and can be done using various methods. These methods include the use of condensation plates, desiccants, and biomimicry. At the heart of every AWG system is a mechanism to create a phase change from water vapor to liquid water.

Historically, passive fog fences were employed using vertically oriented canvas to capture liquid water from humid air [1]. Most modern AWG systems use some form of condensation or desiccants. Modern condensation-based AWG systems generally employ vapor-compression refrigeration (VCR) to extract liquid water.

The AWG methodology proposed in this research is to utilize Peltier (thermoelectric) cooling to achieve optimized AWG rates by maximizing water generation and minimizing power consumption. Peltier cooling is far less efficient than VCR cooling systems, but it has several advantages. These advantages include low-maintenance, high-reliability operation, and the ability to use renewable power resources such as solar. These are all advantageous for regions of the planet that are remotely located and lacking in infrastructure to accommodate higher maintenance and lower reliability VCR systems.

Various heat transfer mechanisms, including conduction, convection (natural and forced), and phase change will be evaluated and optimized. A systematic approach using a configurable AWG test platform will be used to characterize and optimize these various cooling techniques. Additionally, computer thermal/fluid analysis will be performed

using computational fluid dynamics (CFD) simulation.

I. INTRODUCTION

1.1 *Atmospheric Water Generation*

Fresh water is one of the basic needs of humankind. Ensuring an adequate supply of drinking water for all of the world's seven plus billion residents is becoming more challenging each passing year. Therefore, we can expect the challenges involved with ensuring an adequate fresh water supply in the decades ahead will be even more difficult to overcome.

Traditional fresh water supplies utilized historically include lakes and streams, rivers and reservoirs, ponds and creeks. Additional sources include groundwater, rainwater harvesting, and desalination.

In more recent years, other freshwater extraction approaches have been implemented. These include passive dew collectors, gas separation membranes, and atmospheric water generation [2].

There are several methods available for extracting freshwater using AWG techniques. These include active water collection, and passive water collection systems. Active systems include refrigerant-based cooling and thermoelectric cooling systems. Passive systems include surface wettability approaches using hydrophobic and geometrical surface features, as well as thermoregulation techniques. [3]

1.2 *Motivation*

In many places around the globe, limited access to fresh drinking water is more common in locations that also have limited access to reliable utilities and infrastructure such as electricity, waste water treatment, and transportation. Providing access to fresh

drinking water using commercial AWG systems can be challenging due to this lack of infrastructure. Commercially available AWG systems using vapor-compression refrigeration (VCR) cycle power can provide useful amounts of drinking water, but require access to a reliable power grid. Additionally, passive dew collection and gas separation membrane systems can require high maintenance.

Therefore, my approach is to investigate the systematic design of an optimized AWG system that can run on power from a solar panel and battery backup system using thermoelectric coolers. I believe this will provide a low maintenance, high mean-time between failure, sustainable solution for this ever-increasing search for sources for fresh water.

1.3 *Research Objectives*

Using a systematic combination of computational fluid dynamics simulation and related verification testing to correlate the numerical results can result in an optimized design to produce a high rate of water collection for a limited amount of energy expended.

II. DETERMINATION OF AMBIENT CONDITIONS

2.1 *Psychrometric Chart Overview*

In order to begin an optimization process for an AWG system, you first need to quantify the ambient atmospheric conditions in the region the system is to be installed. If the local conditions are such that there is little moisture in the air or that extracting the available moisture consumes too much energy, the system will not be successful. This will always be limited by the physics of the phase change nature of water.

The parameter that is most important to quantify the effectiveness of an AWG system is water volume generated per unit of power expended over time. This is generally specified as liters of water generated per kilowatt over a period of one hour, thus having units of liters/kW·hr.

The factors impacting this parameter can be grouped into three categories.

Climatic Factors

- Atmospheric pressure
- Dry Bulb Temperature
- Relative Humidity

System Parameters

- Peltier Device Coefficient of Performance (COP)

Condensation Plate Surface Parameters

- Surface Texture and Surface Finish

For this research, the climatic and system parameters will be addressed. That is, the goal will be to reduce the temperature of the condensation plates to a maximum amount with a minimum amount of energy expended. The parameter that will be optimized in this research is the change in condensation plate surface temperature per unit of power

expended over a period of time ($^{\circ}\text{F}/\text{kW}\text{-hr}$). Research on condensation plate surface parameters is an active area of research that will be out of the scope of this research.

This chapter will give some background details about the psychrometric chart in general and the introduction of a novel approach to determine in a quantitative way at what dry bulb temperature and relative humidity the AWG system should be operated.

To quantify the climatic factors, a psychrometric chart will be used. The figure below is a simplified psychrometric chart based on the 2009 ASHRAE Fundamentals Handbook.

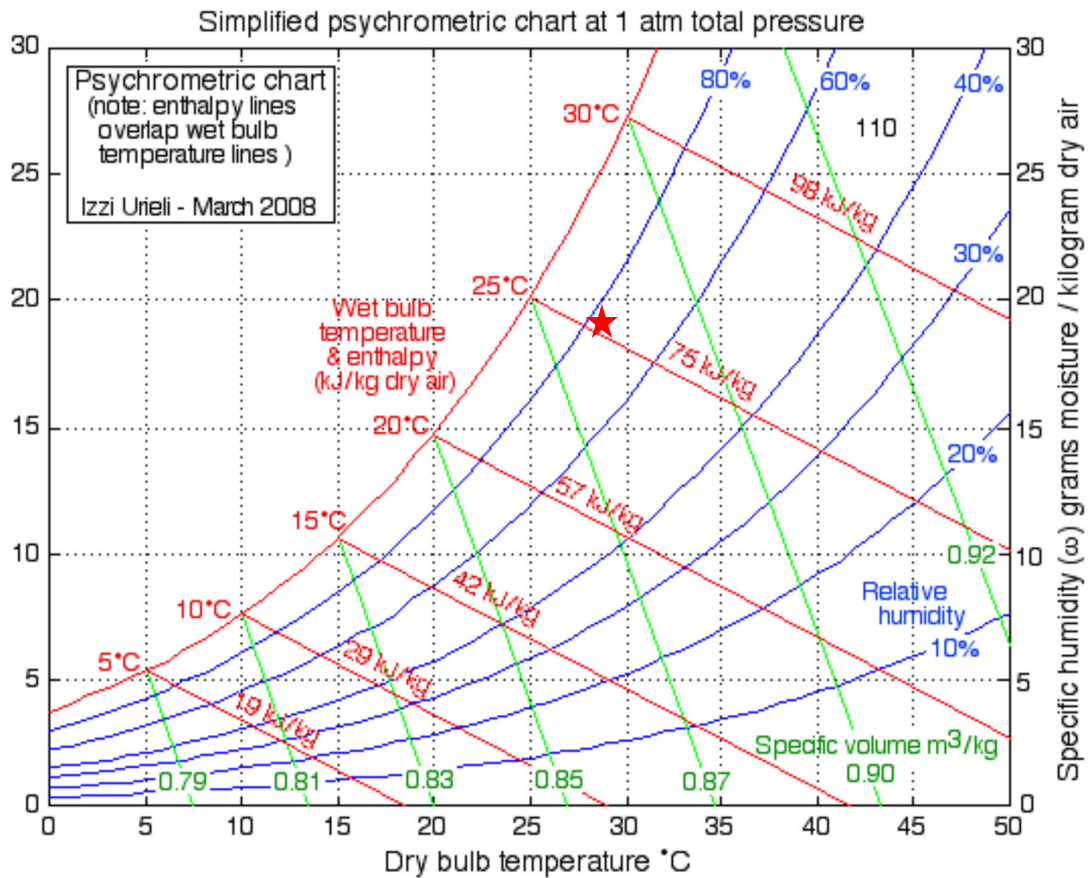


Figure 1 - ASHRAE Simplified Sea Level Psychrometric Chart

This psychrometric chart describes the condition of the air-water vapor at a specific atmospheric pressure. This chart was created for a barometric pressure of 29.921 inches

of Hg (1 atm = 14.7 psi), which is considered standard atmospheric pressure at sea level. For test conditions near San Marcos, Texas, this chart will be used. For altitudes at higher elevations, a modified chart should be used.

2.2 Psychrometric Chart Parameters

Table 1 lists seven separate parameters.

Table 1 - Psychrometric Chart Parameters

Parameter	Units	Description
Dry Bulb Temp	°F	x-axis
Humidity Ratio	lb _{water vapor} / lb _{dry air}	y-axis
Wet Bulb Temp	°F	Measured with Sling Thermometer
Enthalpy	Btu / lb _{dry air}	Measure of Energy in Air and Water Vapor Mixture
Saturation Temp	°F	Dew Point – 100% Relative Humidity
Relative Humidity	%	Ratio of Actual Water Vapor to Maximum Water Vapor
Specific Volume	ft ³ / lb _{dry air}	Amount of Dry Air Present per Cubic Foot of Volume

The chart assumes a constant barometric pressure. The values used in all this research assume a standard atmospheric pressure at sea level. When the system is installed at higher/lower elevations, appropriate compensation should be used.

Being a 2-D chart, specification of any two parameters will fix the remaining five parameters. For most situations, dry bulb temperature and relative humidity are given and the other parameters are determined using the chart.

When comparing atmospheric water generation systems, it is important to compare water

generation rates at a common standard atmospheric condition. The Association of Home Appliance Manufacturers (AHAM) created publication AHAM DH-1-2008 which, among other things, defines a “standard world condition” at atmospheric pressure of 14.7 psi, an 80°F (26.7°C) dry bulb temperature, and a 60% relative humidity. This point is identified in Figure 2.1 with a red star. This condition is set by many AWG suppliers when they test their water generation rates to allow consumers to more intelligently compare water generation rates between different manufacturers and models.

2.3 *Quantifying Optimum Atmospheric Conditions for AWG*

For many places in the world, it can be assumed if money is not a consideration, an unlimited amount of power is available for use for AWG. However, in many places in the world, there is neither an unlimited amount of funds, nor access to reliable power generation. Additionally, these locations are often also short of potable water for human and agricultural use. Therefore, understanding how to best use the limited electrical power available to generate the most amount of water is of utmost importance.

To this end, many experts use a Water From Air Resource (WFAR) index to quantify the suitability of a particular region to provide desirable atmospheric conditions to produce AWG. This parameter is calculated using the same AHAM standard world condition of 14.7 psi atmospheric pressure, 80°F dry bulb temperature, and 60% relative humidity described earlier. Using the psychrometric chart, a specific volume of 13.9 ft³ / lb_{dry air} and a humidity ratio of 0.013 lb_{water vapor} / lb_{dry air} is obtained. Using these values and some conversion factors, a water vapor density at standard conditions is obtained as follows.

$$W.V.D = \frac{lb_{dry\ air}}{13.89\ ft^3} \cdot 0.0132 \frac{lb_{water\ vapor}}{lb_{dry\ air}} \cdot 453.6 \frac{gm}{lb} \cdot 35.31 \frac{ft^3}{1m^3}$$

Therefore, the water vapor density at standard conditions is $15.2 \frac{gm}{m^3}$.

Monthly values of water vapor density for different cities across the globe are averaged and then divided by this water vapor density at standard conditions. This allows overall annual comparisons between cities based on their atmospheric conditions ability to produce AWG in comparison to the standard world condition. Arbitrary grades of WFAR index values have been defined and some sample sites in each of the four categories are listed in the following table.

Table 2 - Water From Air Resource (WFAR) Values

Location	WFAR	Grade
Manila, Philippines	1.27	Excellent
Delhi, India	0.81	Good
Santa Barbara, California	0.59	Fair
Tehran, Iran	0.32	Poor

This method provides for an overall annual comparison of cities across the world that are more conducive to AWG, but it does not allow for real-time analysis of when to operate an AWG system based on current atmospheric conditions.

2.4 *Real Time Evaluation of Optimum Conditions for AWG*

This research proposes a method for the calculation of an alternative index to evaluate local atmospheric conditions for AWG. The same psychrometric chart will be used, and the local conditions (dry bulb temperature and relative humidity) will be identified. For this new index, standard world conditions of 14.7 psi atmospheric pressure, 80°F dry

bulb temperature, and 60% relative humidity will be employed as the baseline.

This condition is assumed as the initial temperature of the condensation plate and surrounding air/vapor mixture (Condition 1). At time $t=zero$, energy is provided to the cooling system which will start cooling the condensation plates. The air immediately surrounding the condensation plates also begins to cool and continues in a sensible cooling fashion (horizontal line on the psychrometric chart until the saturation temperature (dew point) is reached (Condition 2). As power continues to be supplied to the cooling system, the temperature of the condensation plates continues to cool until the condensation plate and surrounding air/vapor mixture reaches a steady-state temperature of 40°F (Condition 3). These three conditions are indicated by the three stars shown in the figure below.

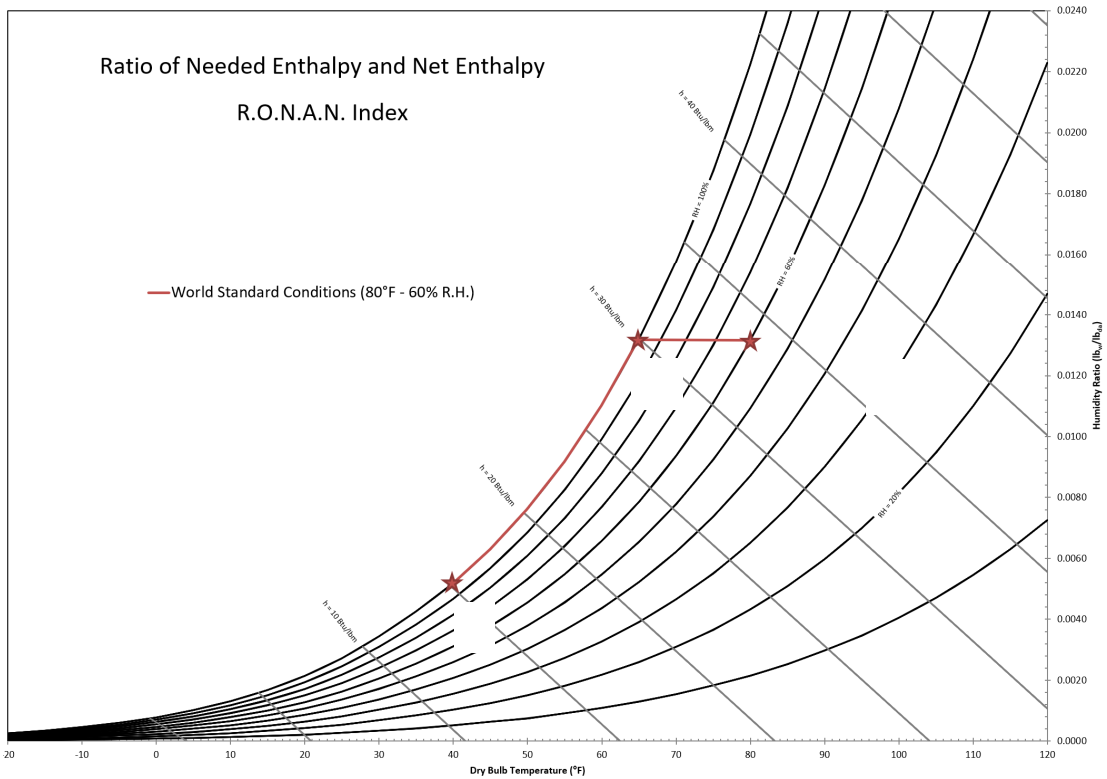


Figure 2 - Ratio of Needed Enthalpy and Net Enthalpy

Next, values for the total enthalpy (energy) of the air/water vapor mixture at each of the three conditions are determined from the psychrometric chart.

Table 3 - Enthalpy Values

Condition	Dry Bulb Temp	Relative Humidity	Humidity Ratio	Enthalpy
1	80 °F	60%	0.013 lb _{water} / lb _{dry air}	33.6 Btu / lb _{dry air}
2	65 °F	100%	0.013 lb _{water} / lb _{dry air}	29.9 Btu / lb _{dry air}
3	40 °F	100%	0.005 lb _{water} / lb _{dry air}	15.2 Btu / lb _{dry air}

Note that as you move from Condition 1 to Condition 2, the relative humidity rises continuously until the dew point is reached, while the humidity ratio remains constant. As you move from Condition 2 to Condition 3, the relative humidity remains at 100%. Between Condition 1 and Condition 2, energy is expended to cool the condensation plates and surrounding air/water vapor mixture, but zero liquid water is generated. Between Condition 2 and Condition 3 is when additional cooling energy is expended, and 100% of the liquid water is generated.

To capture the overall suitability of current atmospheric conditions into a single dimensionless parameter, a novel approach was developed. The ratio of needed enthalpy and net enthalpy (R.O.N.A.N.) index captures the ratio of the change in enthalpy required to create condensation (between Condition 2 and Condition 3) to the total change in enthalpy to achieve 40°F (between Condition 1 and Condition 3). For initial conditions of high humidity and moderately high temperatures, the total energy expended is mostly consumed condensing water as opposed to reducing the initial temperature to the dew point. For initial conditions of low humidity and/or low temperatures, the opposite is

true; most of the energy is expended reaching the dew point rather than actually condensing water. Note that a RONAN index of 1.00 indicates an initial condition of 100% relative humidity and a RONAN index of 0.00 indicates an initial condition of 40°F dry bulb temperature. Initial conditions of less than 40°F have an undefined RONAN index. The equation for calculating the RONAN index is shown below.

$$R.O.N.A.N. = \left(\frac{[enthalpy_2 - enthalpy_3]}{[enthalpy_1 - enthalpy_3]} \right)$$

Arbitrary ranges for the RONAN index have been assigned per the following table.

Table 4 - RONAN Index Value grades

Grade	Index Range
Excellent	1.00 – 0.75
Good	0.75 – 0.50
Fair	0.50 – 0.25
Poor	0.25 – 0.00

Using the midpoints of these index ranges, the following table shows various initial conditions and their associated RONAN and WFAR indices for comparison.

Table 5 - Sample Initial Conditions and Resulting RONAN and WFAR Indices

Grade	Dry Bulb Temp	Relative Humidity	RONAN Index	WFAR Index
Excellent	90 °F	64%	0.88	1.43
Good	80 °F	45%	0.63	0.76
Fair	70 °F	43%	0.38	0.53
Poor	60 °F	50%	0.13	0.44

With limited energy resources to remove heat from the condensation plates to achieve the desired AWG rate, users must be able to identify atmospheric conditions that will result in the most water generation with the least energy expended. Using a psychrometric

chart spreadsheet initially developed by KW Engineering, I have been able to automate the calculation of the RONAN index for any given condition (dry bulb temperature and relative humidity). A link to this Microsoft Excel spreadsheet can be accessed at www.engr1304.com. Based on every unique situation of available cooling energy, a go/no-go index value can be set and used to automate the AWG system currently deployed.

The figures below show these RONAN index ranges graphically.

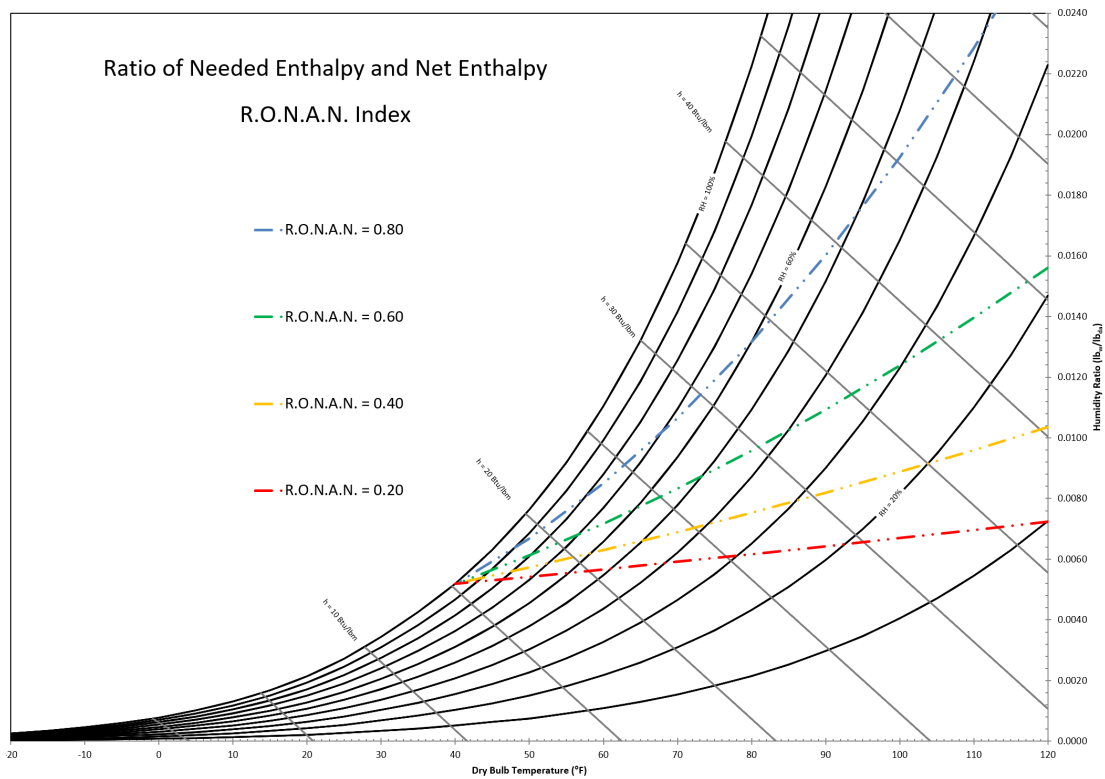


Figure 3 – Constant RONAN Value Family of Curves

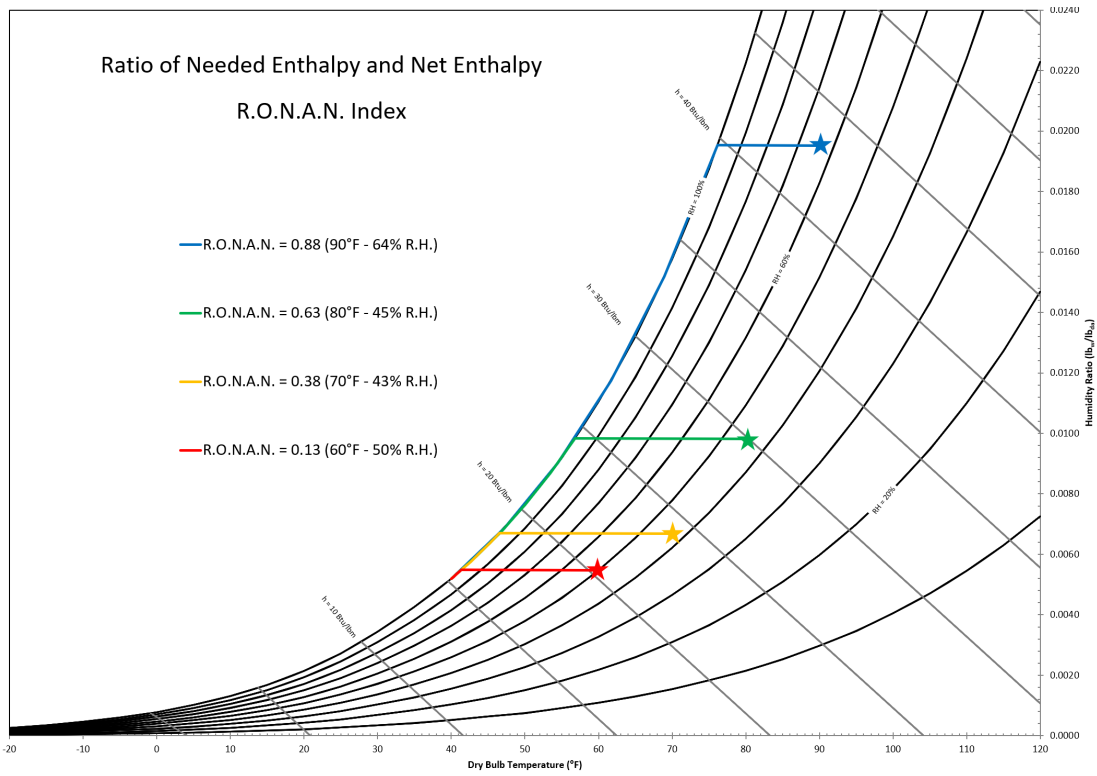


Figure 4 – Range of RONAN Values at Various Ambient Conditions

III. CASE STUDY – SMART AWG

3.1 *Introduction*

Over 1 billion people outside the United States do not have access to clean, safe drinking water [4]. Thousands of women and children spend hours trying to collect water from distant and contaminated places. This means billions of families around the world do not have the ability to drink, cook, or shower with clean water. Water is a basic natural resource, but in reality there is a large shortage all over the world in places such as India, Brazil, South Africa, and Cape Town among others [5].

AWG offers a possible solution to this problem. The condensation that forms on plant leaves and other surfaces can be replicated using an AWG system. Condensation forms when air at the saturation temperature comes in contact with a surface that is below this saturation temperature [6]. AWG systems cause a surface to be cooled and then pass air over it, allowing the moisture to be extracted from the air as it passes. Some researchers have applied biomimetic principles to utilize atmospheric water [3].

Current AWG systems include refrigerant-based dehumidification, vapor compression and vapor absorption refrigeration, desiccant liquid, radiative cooling, thermoacoustic refrigeration, and induced or controlled convection. These systems cannot compete with desalinating other water sources on an energy cost of water basis, because it requires energy to change water from its gaseous state to a liquid state. Current AWG systems require a minimum of 6.8g/m^3 water vapor density and operate ideally at the World Standard Conditions of $26.7\text{ }^\circ\text{C}$ and 60% RH to operate at an efficiency of 0.4 kWh/L [7].

Thermoelectric coolers are a commonly used option for AWG systems. Their low volume, fast response time, and ease of use have made them a popular choice for cooling

systems and have led to the increased characterization of the devices [8]. For systems that use thermoelectric coolers, a relative humidity $\geq 60\%$ and temperatures $\geq 20\text{ }^\circ\text{C}$, is required for the price value and convenient operating range of the system to converge [9]. These ideal atmospheric conditions also help the system avoid frosting over. Outside of these operating conditions, the efficiency of these systems only decreases. In order for AWG systems to be feasible outside tropical environments, steps must be taken to ensure energy is not wasted and the device is kept in the proper temperature range.

This paper presents a study of the development of a smart sensing and control system used to decrease the power consumption of an AWG system by only running it during feasible operating conditions. The system uses a Peltier device, Arduino and simple sensors to determine the energy required to produce water at certain points on the psychrometric chart.

3.2 *Methods and Materials*

The AWG system being examined is constructed using thermoelectric coolers called Peltier devices, in a module that includes a heat sink.

The Peltier devices are thermoelectric coolers that operate by transferring heat between two electrical junctions creating a hot side and a cold side. These devices require a DC voltage and are low maintenance, and controllable.

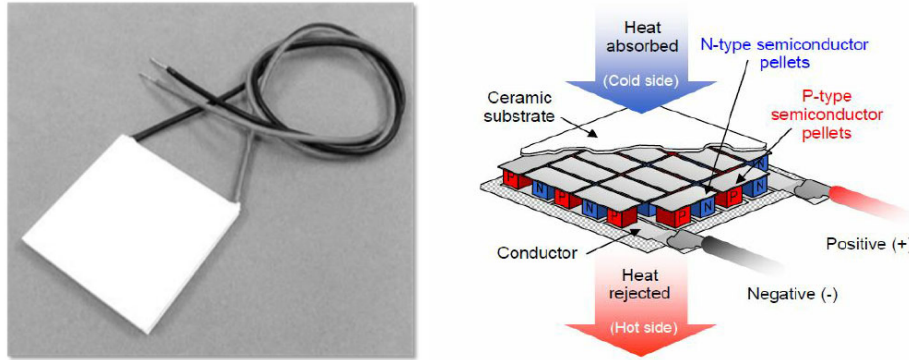


Figure 5 - Peltier Device

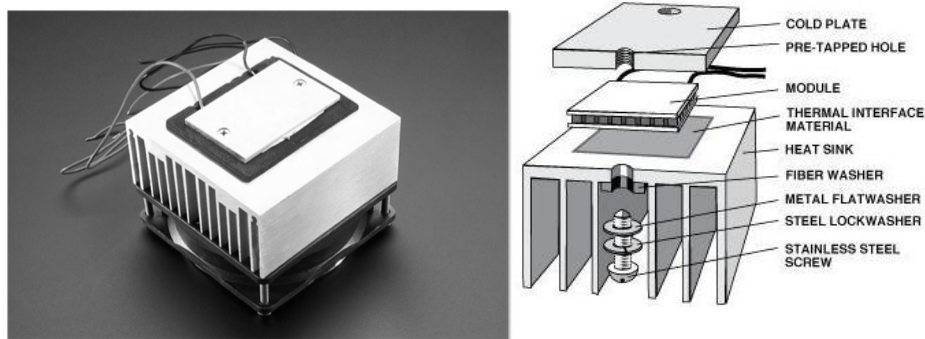


Figure 6 - Peltier Device Module

The Peltier device is 40mm x 40mm and covered by a 40mm x 60mm aluminum plate. The system is rated at 12V 5A, but has been tested at a maximum voltage of 8.5V for this system.

For the system to continually produce water, the aluminum plate on the devices must be kept below dew point, but above freezing temperatures. This requires the device to turn off occasionally, so the water will not freeze, and turn on again as the device approaches dew point. This can also be done by providing a lower current through the device, but this method still leaves the device vulnerable to freezing in lower temperatures and may not be able to cool down enough in warmer atmospheric conditions.

These devices were originally put on a timed cycle so they would not freeze. This method, however, required testing to determine the length of the on and off cycle times.

Different cycle times were also required depending on the power supplied to the system, and the atmospheric conditions. Given that the goal is to create a system suited for different conditions, the timed cycle would cause unnecessary testing and calibration and be also found to be rather ineffective at keeping the device in the ideal temperature range.

At this stage, the smart sensing and control system was implemented. The basis for this system is the Arduino Mega (Figure 3); an inexpensive microcontroller that easily interfaces with multiple sensors including those with an analog output. The relative ease of use makes it possible to test the system with different surface temperature sensors and atmospheric temperature and humidity sensors. The digital I/O pins are used to trigger the relay that turns the device on and off. The Arduino Mega could control up to 17 of the Peltier devices.



Figure 7 - Arduino Mega Microcontroller

The smart sensing and control system uses the Peltier device system shown above, a thermistor, and an Arduino Mega. The thermistor is attached so it touches the center of the aluminum surface of the device. The thermistor is then connected to the Arduino, which takes the analog input of the thermistor and calculates the temperature using the Steinhart equation [10]. When the surface temperature of the device is too cold, the device is turned off using a relay controlled by the Arduino until it warms up again.

This system was significantly more efficient than the timed cycle, yet is still cost effective and, once implemented, can run independently.

3.3 *Psychrometric Analysis*

Through a database obtained from a device that reads the environment conditions every five minutes of the day, an analysis was made in order to determine the best operating conditions at which the system should operate. We refer to “best conditions” as the conditions that minimize the amount of energy consumed and maximize the production of water. With a total of 7,000 data points per month per year, it was attempted to find a trend in the final graphs in order to check in which months the system would be most efficient.

The inaccuracy of this method due to the high variability of environmental conditions over time that derives from external factors such as global warming led to another method to make the analysis.

The psychrometric chart is a visual representation of the atmospheric dry-bulb temperature, relative humidity and dew point at these conditions, and the amount of water in the air at these conditions. This chart allows the enthalpy (energy) to be calculated when moving from state A (initial temperature) to state C (final temperature). For this analysis, state A and state C were selected as conditions were moving from A to C resulted in a difference in humidity ratio of 0.005 lb. of water/lb. of dry air.

When starting at the World Standard Conditions defined earlier, the enthalpy from state A to state C was found to be 13 KJ/Kg. This calculation was performed for multiple points on the psychrometric chart. The calculated enthalpy required from state A to state C was then compared to the enthalpy required when starting at the World Standard Conditions.

3.4 Results

In comparing the smart sensing and control system to the timed cycle, it is valuable to look at the time the device spent in the desired temperature range, above the dew point, and below the desired range. These times are compared in Figure 5.

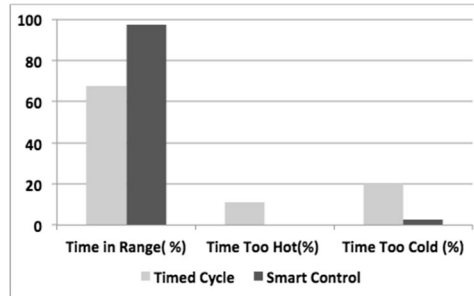


Figure 8 - Timed Cycle vs. Smart Sensing

In a 20-minute trial run, the timed cycle system spent 67.65% of the time in the desired range whereas the smart sensing and control system allowed the device to be in the desired range 97.33% of the time. The “Time Too Hot” represents the time the device was above the dew point and therefore not producing any water. The “Time Too Cold” represents the time the device spent below freezing where energy was wasted because water could not be condensed but the system was still running.

Referring back to the method using the psychrometric chart to obtain the feasible areas, the shape coding was determined the following way: ratios of enthalpy from state A to state C to the enthalpy when starting at the World Standard Conditions between 1.2 - 1.4 are considered ideal conditions (triangle), 1.0-1.2 are low-efficiency conditions (square), 0.8- 1.0 are non-ideal conditions (dashes), and 0.6-0.8 are unsuitable conditions (circle).

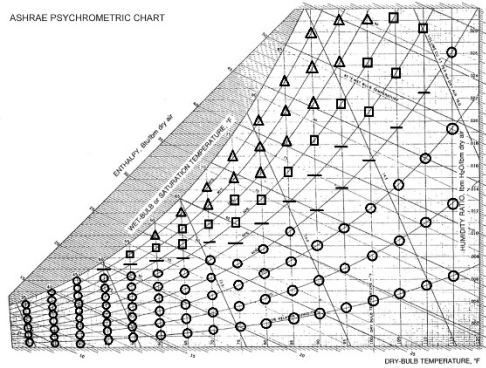


Figure 9 - Operating Condition Ratios

3.5 Discussion and Conclusion

The significant increase in the time the Peltier device spent in range using the smart sensing and control cycle can be attributed to the temperature sensing feedback loop. The small amount of time spent out of the desired range could be a result of the time interval between taking readings from the thermistor. This could be improved by decreasing the time interval between readings or setting a temperature range slightly smaller than the actual desired range. Future improvements to this system involve selecting more accurate temperature sensors and expanding the system to handle multiple Peltier devices at the same time. The sensors to be tested include thermal ribbons and infrared sensors. The infrared sensors would be particularly desirable because they would not need to be in contact with the surface and therefore would not interfere with water collection.

An atmospheric temperature and humidity sensor will also need to be integrated into the system. At this time, the results of the comparison of the World Standard Conditions to the atmospheric conditions can be used to determine if the system should be run. From here, the effect of the atmospheric conditions on the power consumption of the system can be examined with actual data from the system. The power consumed in kWh to run the device in different environments can be compared, and the kWh/L of water

produced at different atmospheric conditions can be calculated.

By determining how and when to run the Peltier device system, the efficiency of atmospheric water generators that use thermoelectric coolers can be increased. The information about which atmospheric conditions to run the device at can also be integrated into existing AWG systems.

IV. IMPROVING HEAT TRANSFER IN AWG

4.1 *Introduction*

Meeting the growing water demand is proving to be one of the most critical challenges of the century [11]. The African Wildlife Foundation estimates that people need 20 to 50 liters of clean water daily to meet their basic needs and in emerging economies, women spend 40 billion work hours each year walking to collect freshwater [12]. Even in developed countries, the increased industrial and agricultural use of water that often comes from freshwater sources has created an urgent demand for other sources of freshwater [13]. Unfortunately, the naturally occurring freshwater sources are not replenished at a rate to match the growing demand. The need for water also comes with a high energy demand, which, in turn, comes with its water demand. The water demand cannot be studied or met without also considering the resulting energy demand. Energy is required to pump, heat, treat and cool and deliver water [14]. Many options exist to help increase the supply of water to these areas in need. Desalination of seawater, the building of aqueducts to transport water from areas with more abundant water supplies, and over-the-road transport of water from one region to another are all possible options, but require infrastructure that might not be in place. Other options include commercial AWG systems, but these require an infrastructure of reliable power to make it happen. AWG offers a sustainable option to secure freshwater for years to come [15]. AWG is expected to be an \$8 billion market by 2024 [16]. AWG is the process of removing and collecting water vapor from the air. Condensation forms when air at the saturation temperature comes in contact with a surface that is below this saturation temperature [17]. AWG systems cool a surface and then pass air over it, allowing the moisture to be

extracted from the air as it passes [18].

AWG systems can rely on a wide array of cooling techniques. Standard systems use refrigerant-based dehumidification, vapor compression, and vapor absorption refrigeration or desiccant liquid. Recently, other methods such as Thermo-electric cooling and heat exchange using lower ground temperatures have been studied [19]. All of these cooling techniques that make AWG possible require power. Current AWG systems require a minimum of 6.8 g/m³ water vapor density and operate ideally at the World Standard Conditions of 26.7 °C and 60% RH to operate at an efficiency of 0.4 kWh/L [20]. In the meantime, the economic aspects of the AWG systems and the feasibility of their usage compared to other sources of freshwater have been studied [20, 21, 22]. The techniques and methods that improve the efficiency of such AWG systems in producing more water with less energy is an area of interest for scaling these methods from laboratory scale to commercial and widespread use.

One of the methods of AWG systems is to use DC-powered Peltier devices (thermoelectric coolers) to reduce the temperature of condensation plates to extract water from the air. This solution eliminates the issues with traditional industrial AWG systems since the Peltier devices are solid-state, have very long mean-time between failure (MTBF) performance, and can be powered by solar panels that eliminate the need to burn hydrocarbon-based fuels or have access to a reliable power grid. Also eliminated is the need to use chlorofluorocarbon (CFC) or hydrochlorofluorocarbons (HCFC) refrigerants that have been shown to deplete the ozone layer. However, thermoelectric coolers have relatively low efficiency. Vapor-Compression Refrigeration (VCR) systems as used in many residential and commercial buildings offer much better efficiency. However, they

have many moving parts (not solid-state), have lower MTBF, and require reliable sources of alternating current. They also require refrigerants that have been proven to cause damage to the earth's atmosphere. Additionally, the thermoelectric cooler device operates on the Peltier effect. The device can accept DC as input and produce a delta temperature as an output (Peltier), or can accept a temperature difference as input and produce a DC as output.

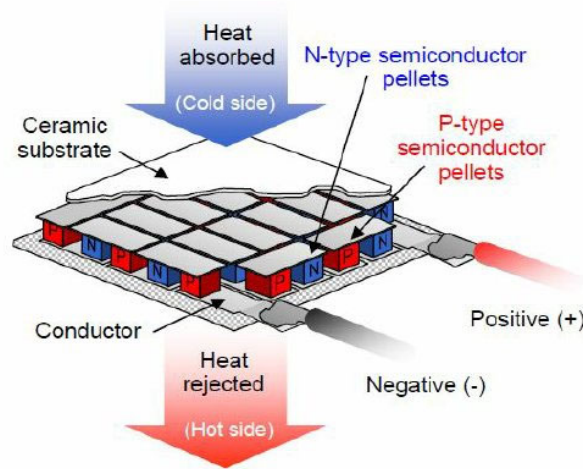


Figure 10 – TEC Operational Illustration [23]

A major challenge with Peltier devices is providing adequate cooling to the hot side of the device. The device can only produce a temperature difference (ΔT). The idea is to attach a condensation plate to the cold side to condense atmospheric water out of the available air to produce water. To minimize the power needed, the challenge is to remove heat from the hot side in an efficient manner to maximize water generated per watt-hour energy expended.

This paper will present methods to improve the efficiency of the thermoelectric coolers

by more efficiently extracting heat from the hot side of the device. The rest of this paper is organized as the following. In section 3, methods and materials including modelling and manufacturing are presented. Section 3 illustrates the results including the simulation model and fabricated test system. Conclusions and discussions are presented in Section 4.

4.2 *Methods and Materials*

Laws of nature constrain us to the fact that heat will naturally move from hot objects to cold objects. Physics provides us with four basic methods to move heat in the opposite direction: Convection (solid material as a medium), Conduction (gas/fluid as a medium), Radiation (via electro-magnetic radiation), and Phase Change (solid-to-liquid-to-gas).

This work has employed all but radiation techniques to systematically determine the best combination to optimize the temperature reduction of the hot side of the Peltier devices.

The approaches used are as follows.

- Convection: Round aluminium finned heat sinks of various lengths
- Conduction: DC tube axial fans blow air across these heat sinks
- Phase Change: Copper wicked heat pipes with distilled water under vacuum

An initial AWG test system included a platform with (4) single commercial 40mm X40mm TEC assemblies cooled with rectangular aluminium heat sinks (conduction) and DC fans (convection) and the system was tested for its efficiency. The results illustrated that the heatsink mechanism is not efficient enough and the system is not getting cold enough in an energy-efficient fashion to produce water economically. As a result of this initial testing, two new approaches were implemented.

a) Increase surface area of the condensation plates.

b) Improve heat transfer away from the hot side of the TEC.

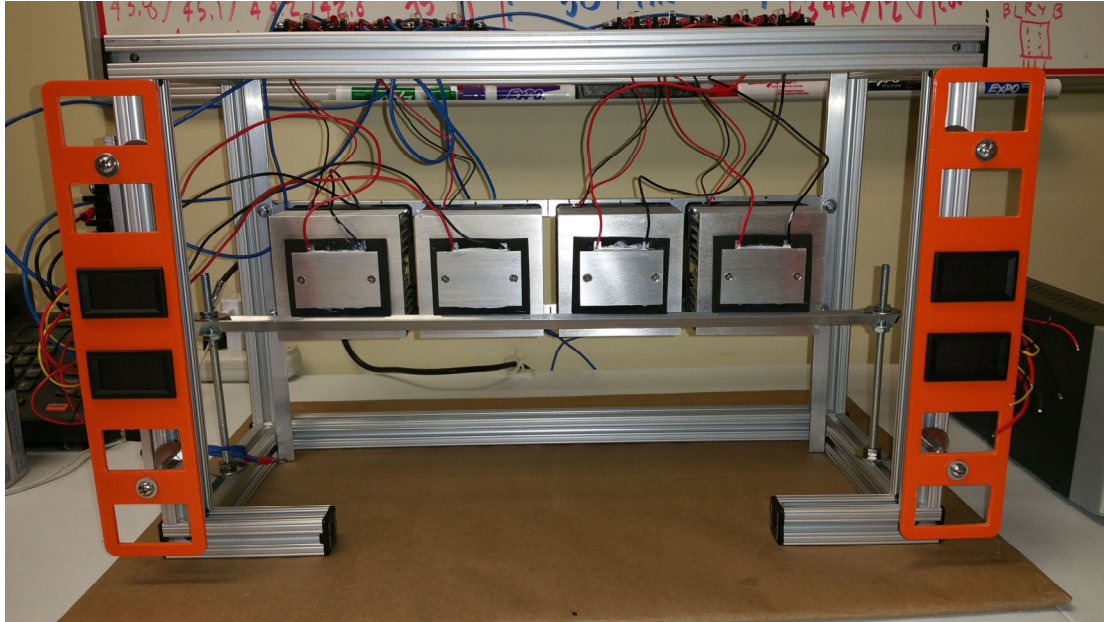


Figure 11 - Original Four TEC Platform

To improve the system, parallel modelling/simulation and Fabrication/Experimentation approaches were pursued to optimize the system. This study focuses solely on the Modelling and Simulation aspects of the work.

4.3 *Modelling and Simulation*

Solidworks software was used to develop a computer model of the system (Figure 3) including the TEC, heatsink, fans, and other mechanical structures. Additionally, Solidworks built-in Flow Simulation was used to implement Computation Fluid Dynamics (CFD) modeling.

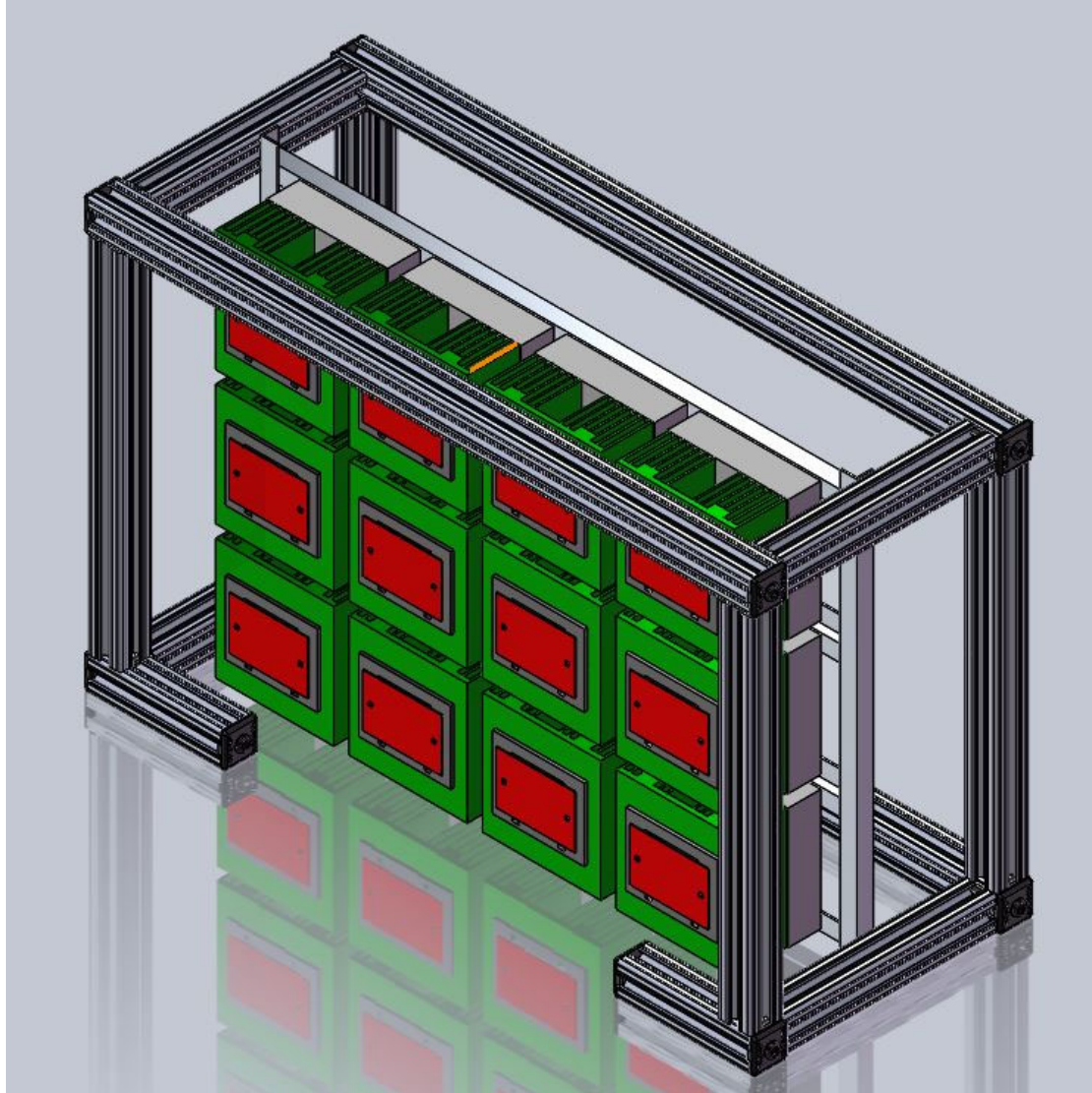


Figure 12 - Original (12) TEC Platform Isometric View

This new improved test platform was about double the size of the original test platform. It contains (4) 8-1/2" x 8-1/2" x 1/8" aluminum condensation plates, (4) 235 cubic feet per minute (cfm) cooling fans, and varying arrangements of one, two three, and four TEC configurations. Also added were spiral ducted air plenums to more efficiently direct the airflow over the new round heat sinks. Four different configurations of heat sink/heat pipe assemblies were designed and manufactured to test the hypothesis of using various combinations of multiple heat transfer mechanisms to optimize the water generation

results.

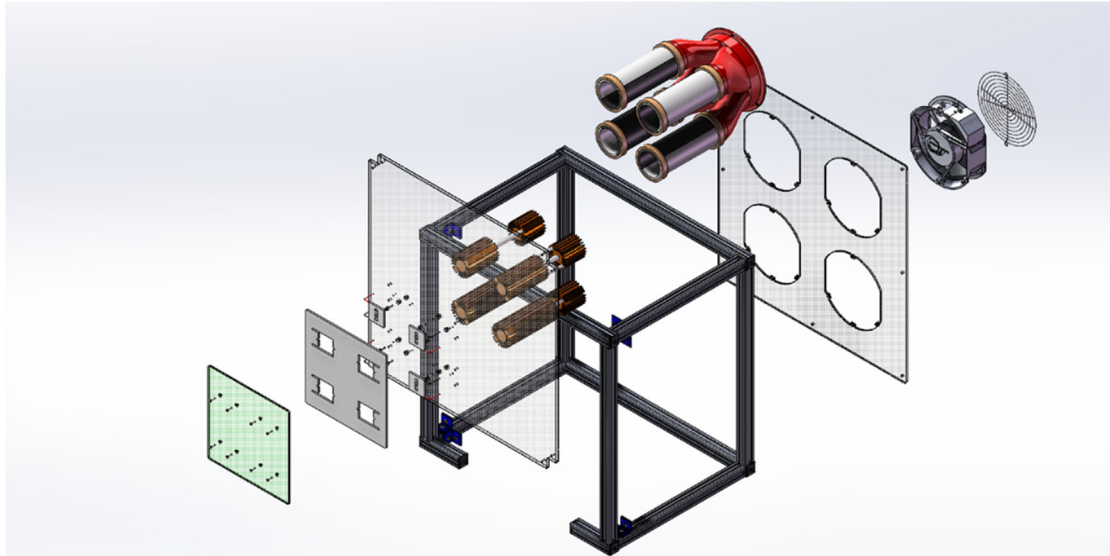


Figure 13 – Updated Test Platform Exploded View



Figure 14 - Hybrid Heat Sink / Heat Pipe Cooling Assembly

4.4 *Results*

The improved AWG Test Platform proved to be much better than the original. The individually configurable condensation plates will allow multiple arrangements of TECs and consistent test results. The CFD analysis that was done closely matches the actual

hardware temperature performance, which will allow for much quicker “what-if” simulations without building additional hardware. Examples of data correlation between the CFD analysis and testing include the temperature gradients seen across the condensation plates. The steady-state temperature from the CFD analysis correlated well with the thermal camera imaging.. Additional specific details of the analysis results are discussed in Chapter 8.

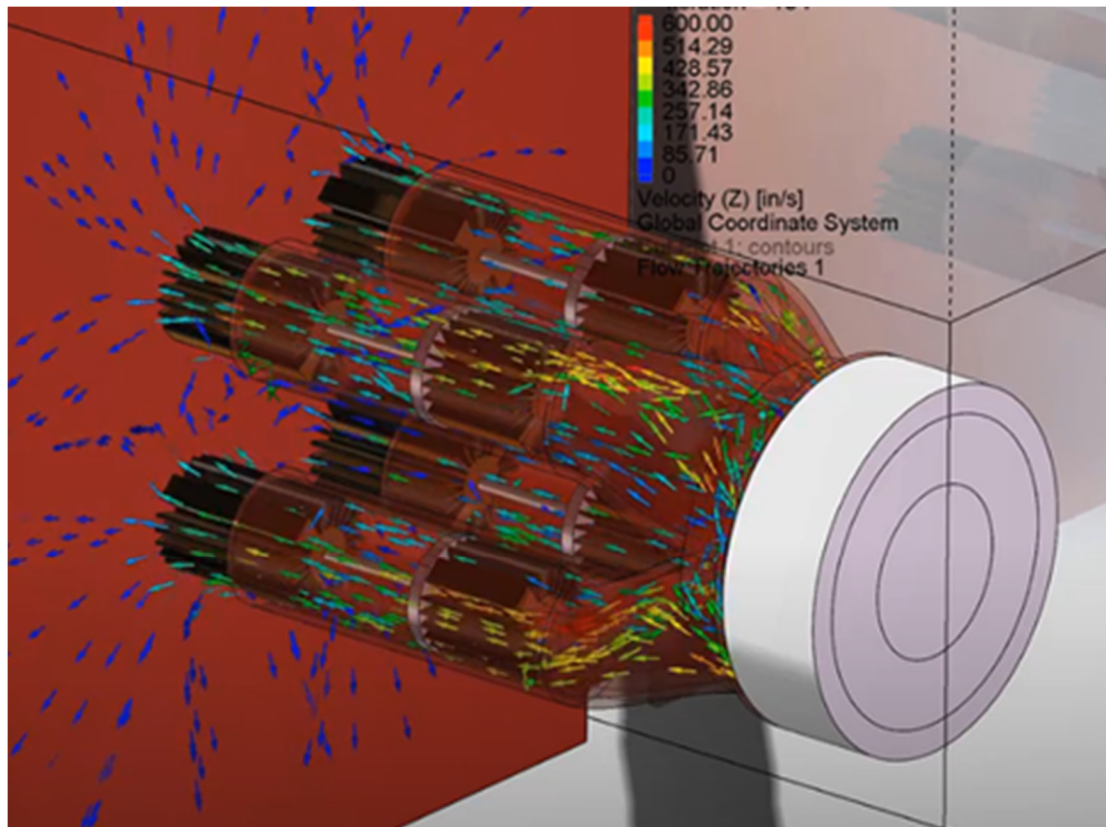


Figure 15 - Computation Fluid Dynamics (CFD) Simulation of Four-Way Duct Design

Adding the heat pipes offered marginal benefits on the initial testing. However, additional configurations are using larger diameter heat pipes that still need to be manufactured and tested. Bluetooth temperature sensors allow temperature probing of the surface of the heatsinks, hot and cold sides of the TECs, and airflow temperature. Airflow sensors allow validation of the results of the CFD analysis, which further

strengthens the ability to perform “what-if” design changes to the duct geometry for design iteration improvements without the need for time-consuming and costly fabrication of intermediate design improvements.

4.5 *Conclusion and Discussion*

CFD Simulation and validation results were very close to actual measured values. This valid model will facilitate a wide range of design of experiments tests and optimizations without the need to fabricate physical models.

Due to the scalable design of the AWG test platform, once the initial design achieves an adequate level of optimization, multiple copies of the test platform can be manufactured into a unit suitable for field tests. A separate optimized solar panel system is also being designed and tested for potential use as a power source for the AWG system.

The Peltier devices are still operating at a sub-optimal coefficient of performance (COP). Ideas for increase optimization include heat sinks with a higher number of thinner fins, investigation of additional TEC arrangements (new spacings and quantities), incorporation of computer-controlled power inputs based on local atmospheric conditions (dry-bulb temperature, atmospheric pressure, and relative humidity).

V. AWG DESIGN PARAMETERS

This chapter will identify the parameters being evaluated to determine the optimum design for the AWG system. These parameters are listed below.

- Peltier devices (Laird 199 coupler and Generic 127 coupler TECs)
- TEC grid configurations (one, two, three and four grid configurations)
- Air duct configurations (one, two, three and four duct plenum configurations)
- Radial aluminum heat sink lengths
- Number, diameter, and lengths of copper phase transition heat pipes

Based on the need for an AWG system that can be used in remote locations with potentially limited access to utilities, provide a low maintenance solution, and be environmentally friendly, the following base features were chosen.

- DC power to operate the system
- Thermoelectric coolers (Peltier device) to provide heat transfer mechanism for cooling
- Axial fans to provide forced convection cooling
- Aluminum heat sinks and condensation plates for efficient conductive heat transfer
- Hollow copper heat pipes containing distilled water under vacuum to supplement forced convection cooling with phase change cooling mechanism

Using DC power will allow the use of solar panels and a rechargeable battery system to power the unit when placed into service. This will alleviate the necessity of having reliable access to a traditional AC power grid. Although a vapor-compression refrigeration (VCR) system is more efficient than a thermoelectric system, the

thermoelectric cooling system has the added benefit of higher reliability, lower maintenance, and less environmental impact since no potentially ozone-depleting refrigerants are required. The Peltier devices used have no moving parts and no maintenance requirements like traditional VCR systems, and have mean-time between failure (MTBF) reliability approaching 300,000 hours.

5.1 *DC Power*

To provide adequate power to the TECs and cooling fans, eventually a combination of solar panels and a battery storage system will be utilized. However, during system testing, traditional benchtop DC power supplies will be utilized.

For the fans, 12V nominal voltage will be provided and the fans will pull the amount of current required to overcome the back pressure of the system. For the TECs, they will provide a preset current and allow the voltage to fluctuate depending on the transient operating temperatures.

5.2 *Thermoelectric Coolers (Peltier Devices)*

To move heat away from the aluminum condensation plates, TEC1-12706 thermoelectric coolers were utilized. These units are 40mm x 40mm x 3.8mm in size and are single-stage TECs available from various manufacturers.



Figure 16 – TEC1-12706 Thermoelectric Cooler

The TECs have 127 semiconductor N-P couples and have a maximum operating voltage of 17V and maximum operating current of 6A.

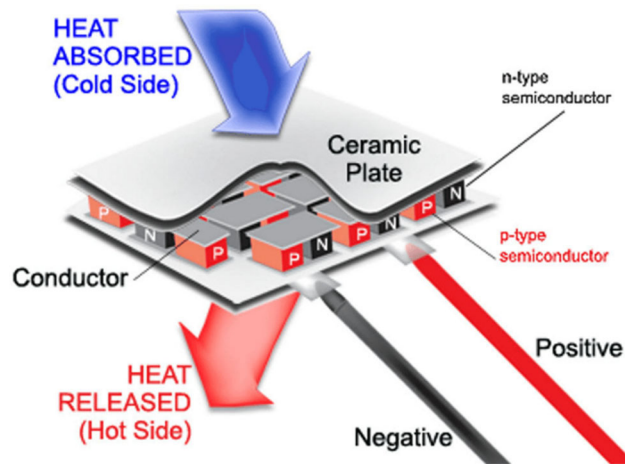


Figure 17 – TEC Component Illustration

The optimization parameter of these devices is measured as the coefficient of performance (COP). COP is defined as follows.

$$C.O.P = \frac{Q_c}{\text{Input Power}}$$

Input power is measured as voltage x current. When operating these devices at high power/voltage, the COP drops off dramatically. Additionally, as the temperature difference between the hot side and cold side increases, the COP also diminishes quickly. It also decreases as the hot side temperature rises. These parameters can be seen in the following family of curves.

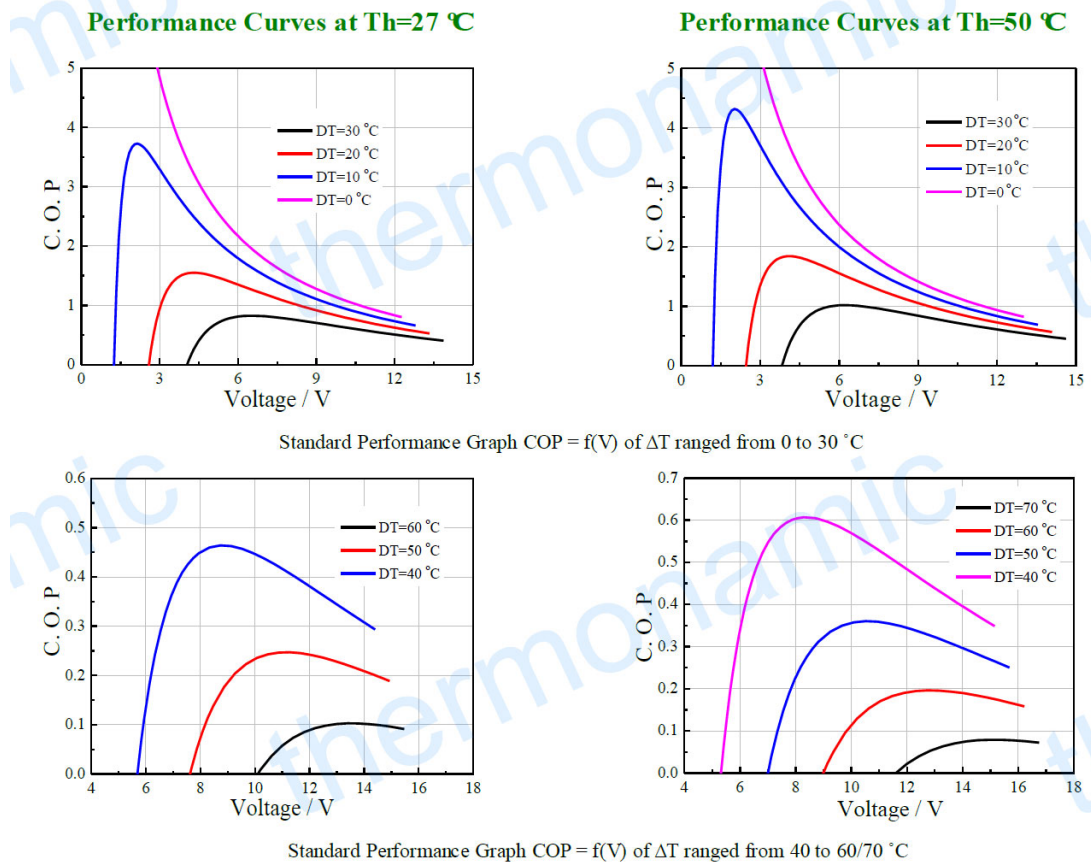


Figure 18 – TEC Coefficient of Performance Curves (<http://www.thermonamic.com>)

5.3 Tube axial Cooling Fans

To reduce the temperature of the hot side of the TECs, DC tube axial fans will be employed. To match the nominal 12V requirements of the TECs, 12V DC fans will be

used. These will direct air through a set of air ducts to blow directly over the heat sinks to increase the forced convection heat transfer rates of the system. The current provided can be adjusted to control the fan rotational speed (and therefore volumetric flow rates) of the fans.

5.4 *Aluminum Condensation Plates and Heat Sinks*

The surface finish of the condensation plates has a major impact on the amount of water that can be extracted from the air at a given temperature/humidity. Additionally, surface features that create hydrophilic and/or hydrophobic enhancements also play an important role. However, for this research, we will use bare .125 thick aluminum condensation plates with a surface roughness between 32 and 64 microinches.

Mounted directly to the hot side of the TEC devices will be extruded aluminum heat sinks. These will be housed inside the extended ductwork so as to concentrate the forced air across the exposed fins.

5.5 *Copper Heat Pipes*

To enhance the heat transfer rates away from the hot side of the TEC, copper heat pipes will be employed. These will move heat through a phase change mechanism of distilled water housed under vacuum inside a hollow copper tube.

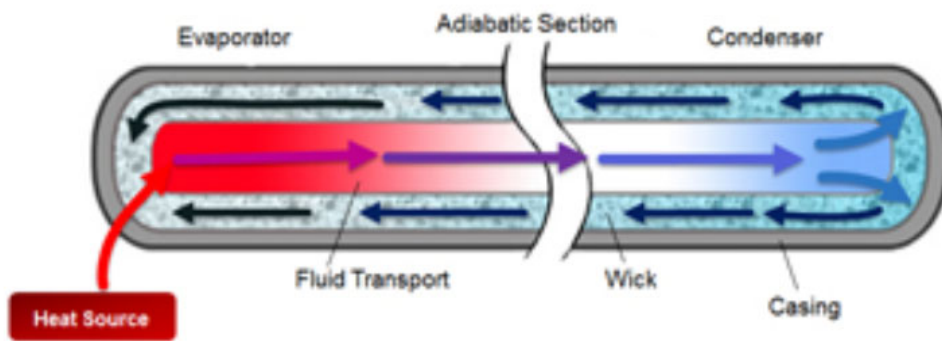


Figure 19 – Heat Pipe Component Illustration (www.qats.com)

These are designed such that the hot end acts as an evaporator and the cool end as a condenser. Since the distilled water is at a low pressure inside the hollow copper tube, it boils at a relatively low temperature, then quickly moves to the cool end, where the water condenses and returns through capillary action through the wicking mesh inside the tube back to the hot end to repeat the cycle.

A large amount of heat is released during this gas to liquid condensation phase change, which will supplement the conduction/convection heat transfer through the heat sinks.

VI. AWG SYSTEM DESIGN

This chapter will explain the design details of the AWG system that will be used as the test platform for experimentation and validation of the models.

The overall goal is to maximize the water collection rate per unit power expended. Since water collection rates are highly dependent on the surface features of the condensation plates, which is beyond the scope of this research, the parameter I will optimize is the energy expended to cool the condensation plates to an average temperature of 40°F. Although lower condensation plate temperatures will result in additional water generation, care must be taken to monitor this temperature closely to ensure it does not approach 32°F (0°C) and result in the condensing water to freeze.

6.1 *Design Parameters*

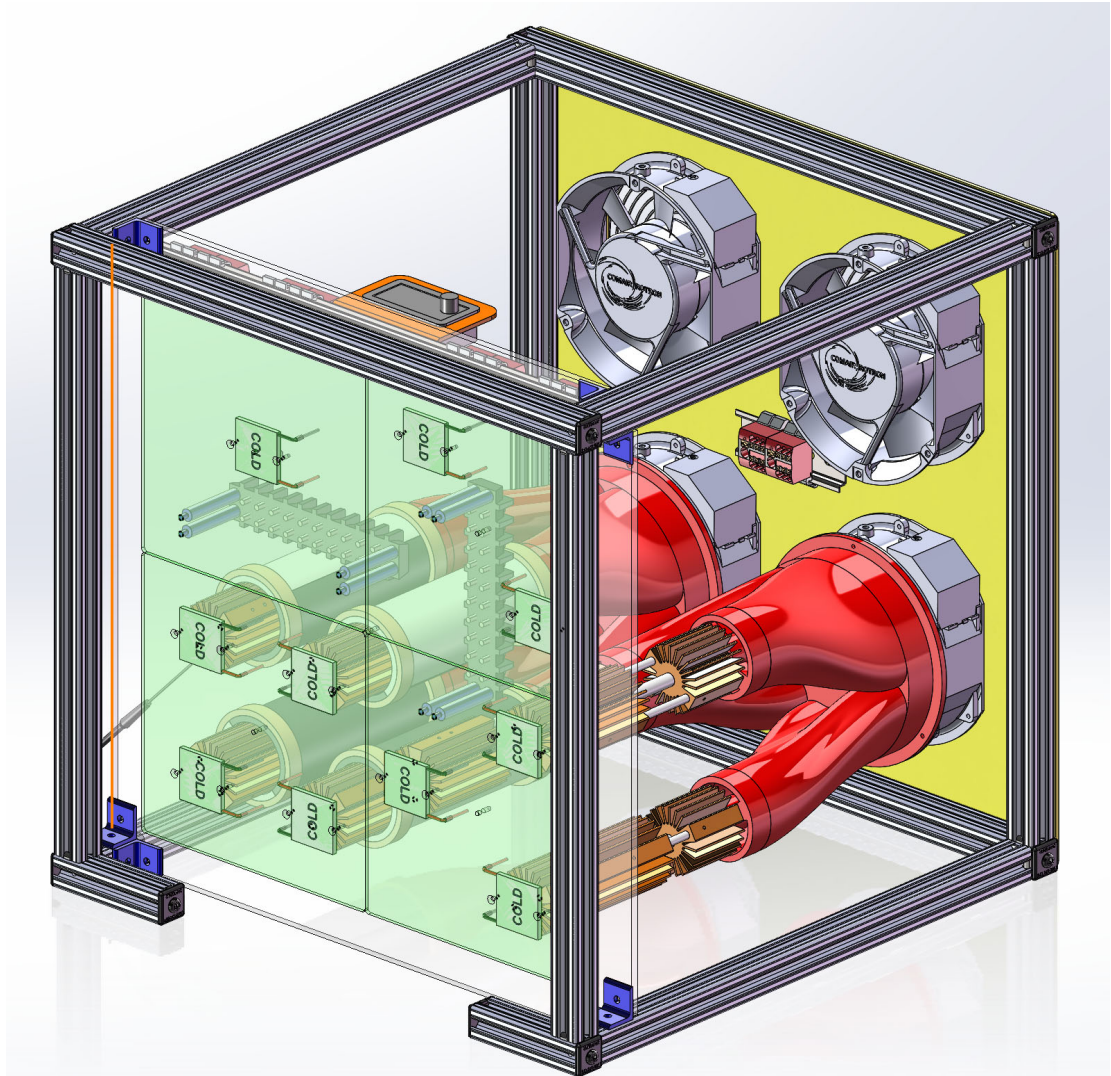


Figure 20 – Final AWG Test Platform

Design variables used to optimize the AWG system are listed below.

- Four geometric configurations (1 – 2 – 3 – 4) of the thermoelectric coolers (Peltier device)
- Four axial fans/duct assemblies to supply cooling air to the four TEC configurations (three duct and four duct versions shown)
- Four different aluminum heat sink / heat pipe length configurations were

employed. This will provide both forced convection cooling and phase change cooling mechanisms.

6.2 Thermoelectric Cooler / Fan Assembly Geometric Configurations

Four different thermoelectric cooler configurations were studied. Each set of TECs are mounted on a separate 8.50” x 8.50” condensation plate. These four condensation plates are thermally isolated from the “hot” side components by use of an 1/8” thick neoprene foam sheet. The TECs are captured within 40mm x 40mm cutouts in this foam.

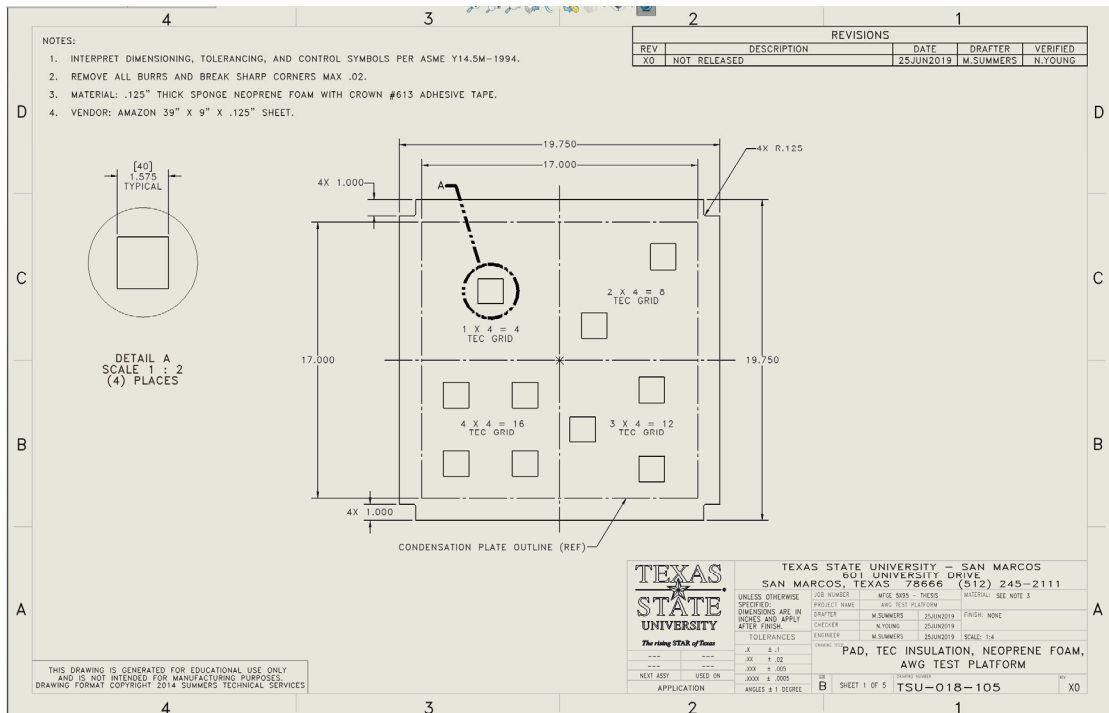


Figure 21 – TEC Grid Configurations

The duct assemblies consisted of a split design. The transition duct directs the air flow from the tube axial fan to the entrance of the laminar flow tube that surrounds the heat sink / heat pipe assemblies. The laminar flow tubes employ a modular design that allows them to be split to gain access to the heat sink / heat pipe assemblies without the

need to disassemble them from the condensation plate assemblies. To gain access to the heat pipe/heat sink assemblies, the two tube rings are slid off the split laminar tubes, which are then separated by disengaging the tab/slot features that hold them together during operation.

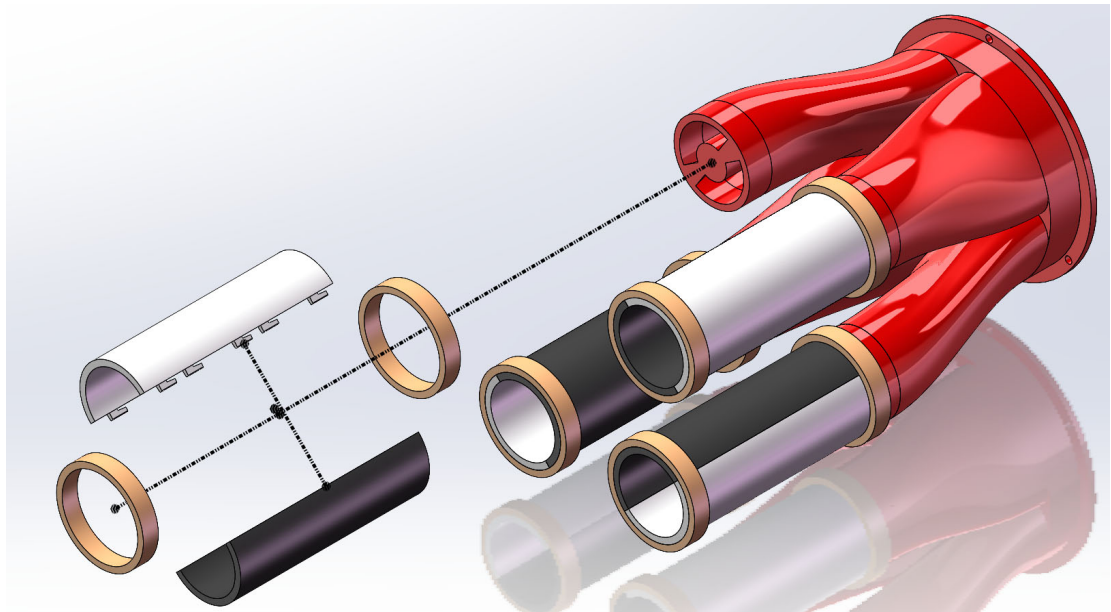


Figure 22 – Cooling Air Duct Design Methodology

6.3 *Heat Sink / Heat Pipe Configurations*

Four heat sink/heat pipe configurations were considered.

Table 6 – Heat Pipe Assembly Dimensions

Dash No.	“Hot” Heat Sink Length	“Cold” Heat Sink Length	Heat Pipe Effective Length
-003	3.00”	2.00”	4.40”
-004	4.00”	2.00”	3.90”
-005	5.00”	2.00”	3.40”
-008	7.87” (200 mm)	N/A	N/A

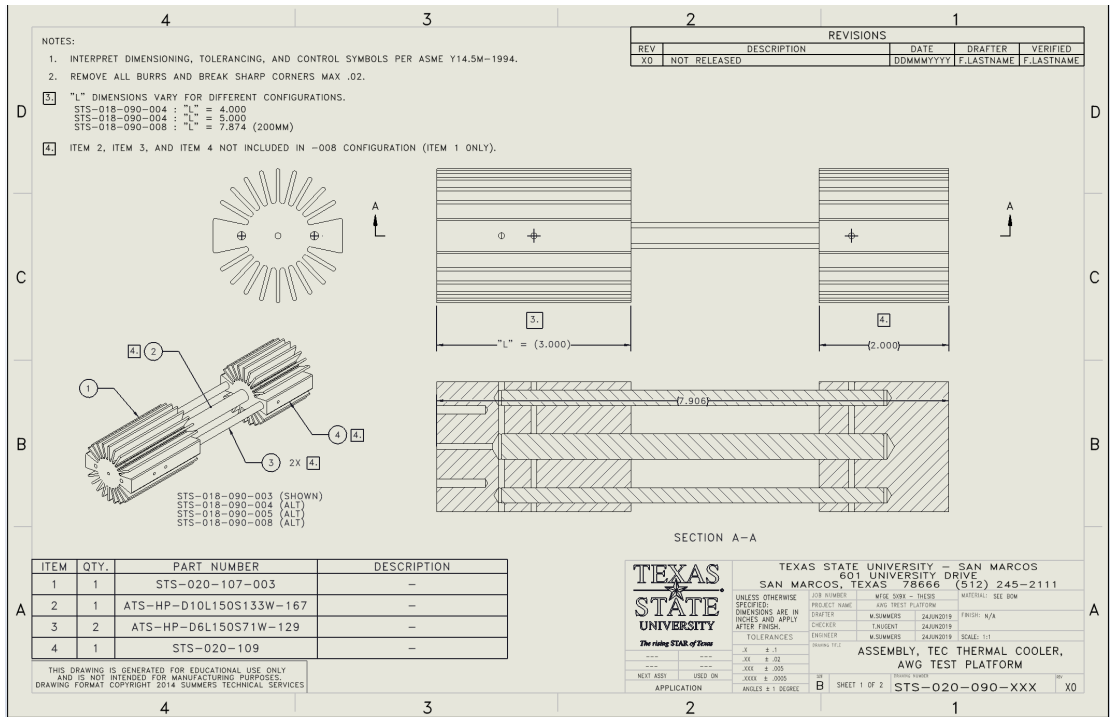


Figure 23 – Heat Sink Assembly Configurations

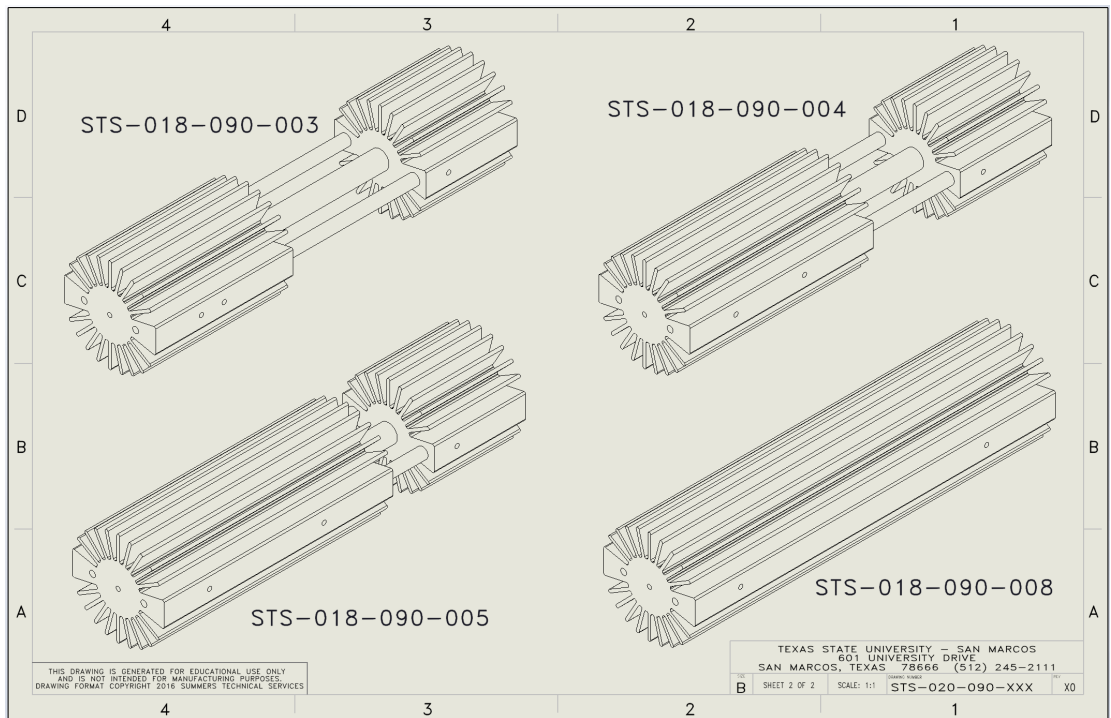


Figure 24 – Heat Sink Assembly Isometric Views

VII. COMPUTATIONAL FLUID DYNAMICS SIMULATION

Using the Solidworks manufacturing model as a starting point, a Solidworks Flow Simulation model was created. To facilitate faster computation times as well as provide adequate mesh fidelity, the overall test platform model was broken up into three separate flow simulation subassemblies. These include the Duct Airflow Sub-Assemblies, the Heat Sink/Heat Pipe Sub-Assemblies, and TEC/Condensation Plate Sub-Assemblies.

Solidworks Flow Simulation is a module embedded inside Solidworks Premium CAD modeling software that allows CFD simulations of existing CAD models. It utilizes the Navier-Stokes equations to extract approximate solution for pressure and temperature values using numerical algorithms. Although the software allows both steady-state and transient analysis, only steady-state analyses were done in this research.

An immersed-body cartesian based mesh algorithm is utilized in the software. Control volumes are created based on mesh size parameters specified in the meshing model. These control volumes can be sized to accommodate high pressure and high temperature gradients as needed.

The control volumes come in three different types.

- Fully solid
- Fully fluid
- Combination of solid and fluid

To accommodate rapidly changing geometry, mesh refinement can be applied to the overall mesh parameters. This can improve the accuracy of the pressure/temperature results where these parameters are changing rapidly with respect to the local geometry.

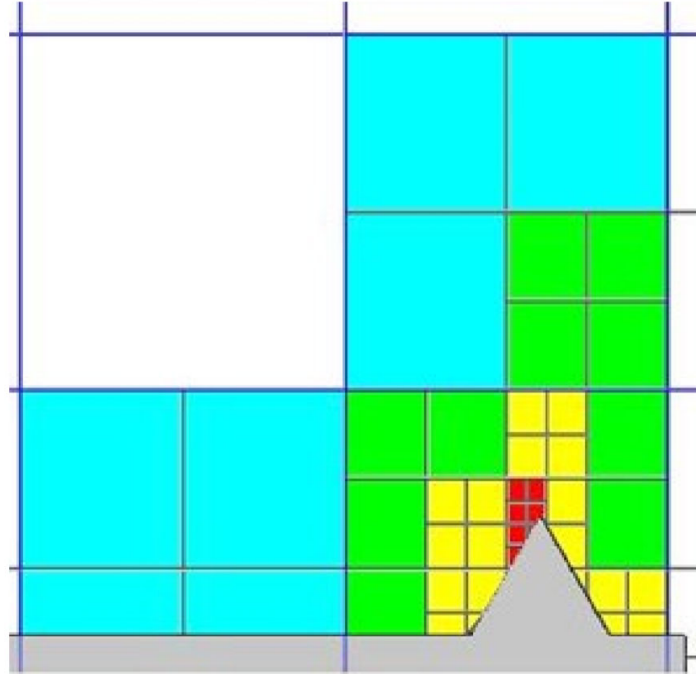


Figure 25 – Mesh Refinement Options [24]

In fluid regions, Solidworks Flow Simulation solves the Navier-Stokes equations, which are formulations of mass, momentum, and energy conservation laws.

$$\frac{\partial \rho}{\partial t} + \frac{\partial(\rho u_i)}{\partial x_i} = 0$$

$$\frac{\partial(\rho u_i)}{\partial t} + \frac{\partial}{\partial x_j}(\rho u_i u_j) + \frac{\partial P}{\partial x_i} = \frac{\partial}{\partial x_j}(\tau_{ij} + \tau_{ij}^R) + S_i$$

$$\frac{\partial \rho H}{\partial t} + \frac{\partial \rho u_i H}{\partial x_i} = \frac{\partial}{\partial x_i} \left(u_j (\tau_{ij} + \tau_{ij}^R) + q_i \right) + \frac{\partial p}{\partial t} - \tau_{ij}^R \frac{\partial u_i}{\partial x_j} + \rho \epsilon + S_i u_i + Q_H$$

$$H = h + \frac{u^2}{2}$$

Figure 26 – Navier-Stokes Equations [24]

In solid regions, Solidworks Flow Simulation calculates heat conduction and joule heating due to electrical currents throughout the system. Although the software has

provisions to accommodate it, in this analysis, joule heating was not employed.

Radiation heat transfer was also ignored due to the relatively low temperatures involved.

External flow type analysis was employed, which entails defining a computation domain that surrounds the components of the design. As a design rule, the computation domain was set to be approximately two times the size of the extent of the CAD model. The fluid was assumed to be air and both laminar and turbulent flow regimes were considered.

Ambient conditions were set at 70°F and 14.7 psia. Ambient airflow was set to zero and all analyses were done using steady-state conditions.

The solid components of the design such as air ducts, heat sinks, insulating foam, and aluminum plates were assigned material properties to model the thermal conductivity of the applicable material. The Comair-Rotron cooling fans were modelled as internal fans, which allowed the manufacturer's pressure vs. volumetric flow rate curves to be input directly into the model. Therefore, based on the pressure drop through the duct system, the appropriate volumetric flow rate was computed.

JQ12B4

Property:

Value	
Volume flow rate	Pressure difference
0 m ³ /s	207 Pa
0.0047 m ³ /s	199 Pa
0.0189 m ³ /s	174 Pa
0.0297 m ³ /s	149 Pa
0.0378 m ³ /s	124 Pa
0.0472 m ³ /s	100 Pa
0.059 m ³ /s	85 Pa
0.0887 m ³ /s	50 Pa
0.1015 m ³ /s	25 Pa
0.1109 m ³ /s	0 Pa

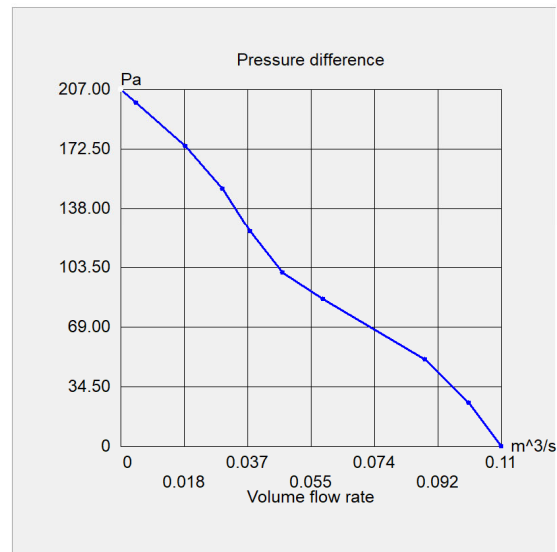


Figure 27 – Fan Curves

For the Peltier devices, thermoelectric cooler elements were employed. Values from the manufacturer's datasheet were input, including maximum pumped heat, maximum delta temperature across the device, maximum current, and maximum voltage. All these parameters were input at the two hot side temperature values provided by the manufacturer, which was 27°C and 50°C for the 127 coupler TEC modules and 25°C and 50°C for the 199 coupler TEC modules. For the output, hot side and cold side average surface temperatures, heat flux through the device, and steady-state voltage values for each TEC were extracted.

7.1 *Duct Airflow Optimization*

To optimize the duct volumetric air flow rates supplying cooling air to the heat sink assemblies, the following CFD model was created.

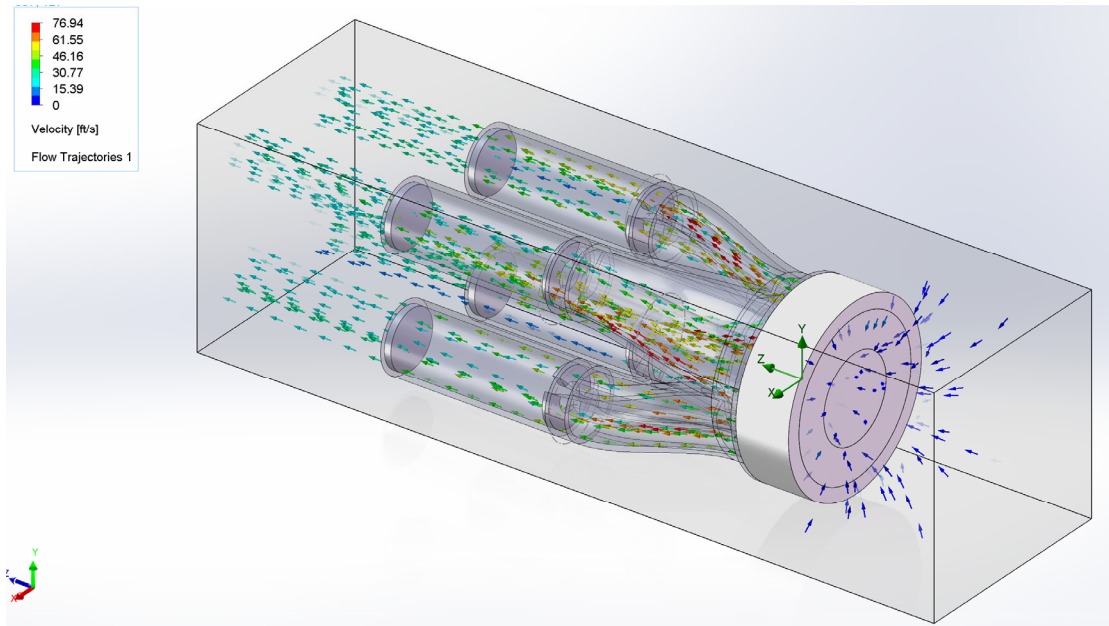


Figure 28 – Duct Air Flow Particle Trajectories

Using the pressure vs volumetric air flow rate curves from the Comair-Rotron JQ12B4 tube axial fan datasheet, an internal fan element was created to evaluate the fan duct design efficiency. Parameters that were optimized included the volumetric flow rate at the duct exit plane and flow percentages through the two halves of each heat sink flow cavity. Three iterations of the duct CAD model geometry were done to ensure a minimum pressure drop / maximum volumetric flow rate through the duct system and even flow rates across both halves of the radial heat sink.

7.2 *Heat Sink Optimization*

Once an optimized duct design was developed, the heat sink assemblies were added to the model to evaluate cooling rates for the different configurations of heat sink/heat pipe assemblies.

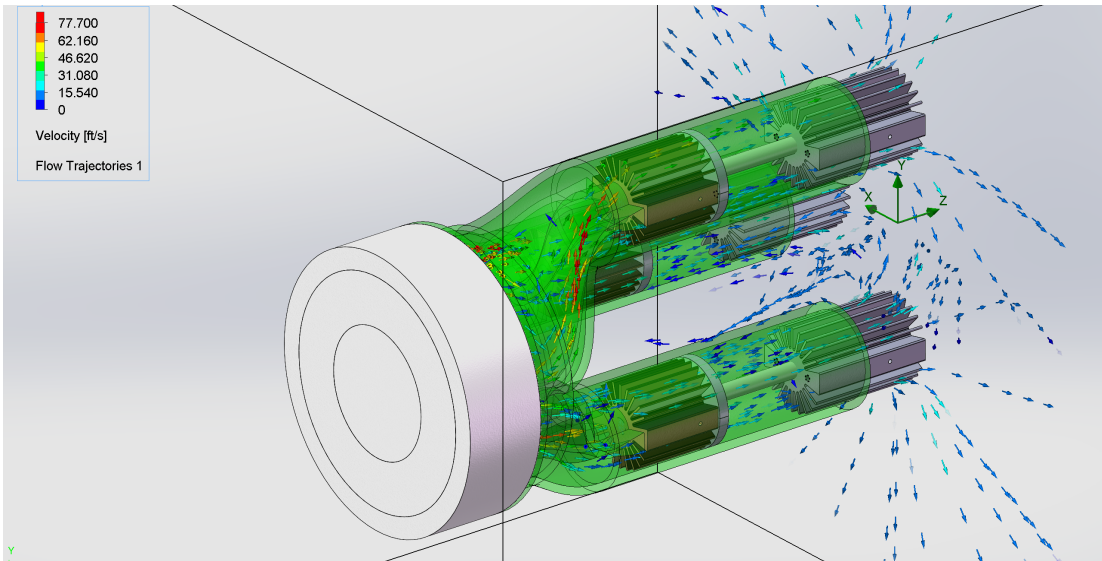


Figure 29 – Duct Airflow with Heat Sink Assemblies

A constant heat flux was placed on the hot plate end of each heat sink assembly to simulate the approximate heat load of the hot side of the thermoelectric cooler. The heat transfer path was through the first heat sink via conduction, then either out through forced convection into the downstream air flow or through the copper heat pipes through a phase change heat transfer mechanism. From there the heat flow continues to move into the second heat sink and then through additional forced convection into the cooler upstream airflow. The various heat sink/heat pipe configurations were tested to determine the optimum design.

7.3 *Thermoelectric Cooler Grid Optimization*

Four different TEC grid configuration arrangements were evaluated. Parameters being optimized include the bulk temperature of the condensation plate surface and the coefficient of performance of the Peltier devices. The Peltier devices were modelled as thermoelectric cooler devices in Solidworks Flow Simulation. Input parameters included maximum pumped heat, maximum delta temperature, maximum current, and maximum

voltage. There were input for the two operating temperature values provided by the manufacturer for the CP14-199-045 (25°C and 50°C) and TEC1-12706 (27°C and 50°C) modules.

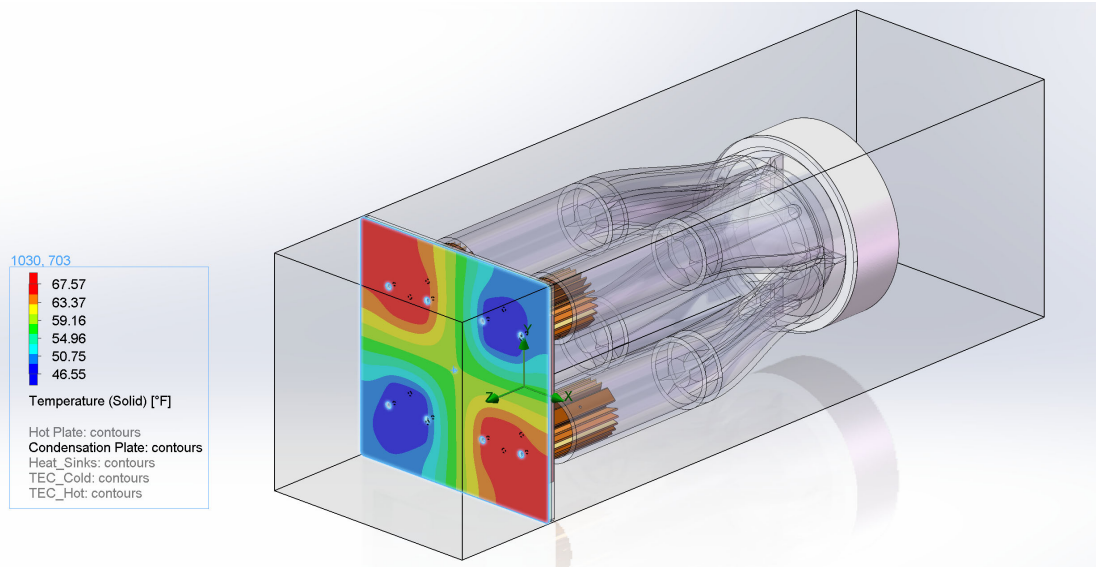


Figure 30 – Condensation Plate Temperature Distribution Profiles

To maintain approximate equal power input to each of the four grid patterns, the simulation was done with equal total input current provided to the four different configurations.

Table 7 – TEC Supplied Current

Number of TECs	TEC Current (A)	Total Current (A)
1	5	5.0
2	2.5	5.0
3	1.67	5.0
4	1.25	5.0

The four TEC grid obtained the best balance of low average condensation plate temperature and lowest temperature gradients. As mentioned earlier, the one and two

TEC grid configurations developed sub-freezing condensation plate temperatures at the TEC locations, which is unacceptable for efficient AWG performance.

Using the FLIR thermal camera, a video was recorded that demonstrated the transient temperature profiles. After about fifteen minutes, the temperatures settled into an equilibrium condition.

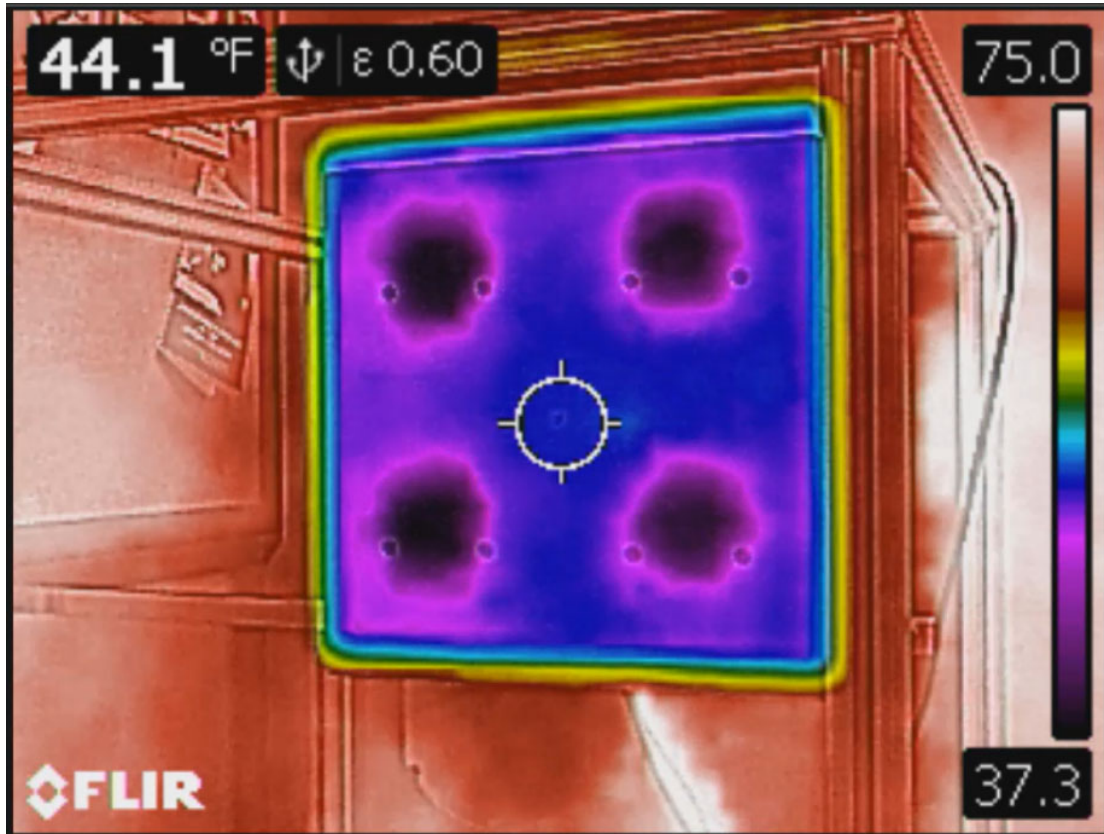


Figure 31 – Condensation Plate Temperature Distribution Profiles

Once the simulation was run, output values for the individual Peltier device input voltage and hot/cold side temperature differences were extracted and coefficient of performance values was determined for each Peltier device using the manufacturer provided performance curves.

VIII. CONCLUSIONS

8.1 *Transient vs. Steady-State Results*

Initially, a transient (time dependent) analysis was attempted to investigate the Smart AWG approach. This was the approach investigated early on, which toggled the power source to the Peltier devices. Since most all of the materials used for heat transfer had high thermal conductivity (aluminum), the temperature quickly returned to ambient after power was removed. It was determined that on/off cycles attempted more than every few hours were not effective.

For the bulk of the analysis, steady-state analysis was performed. This provided quicker run times using the Solidworks Flow Simulation software.

8.2 *TEC Module Types*

Two types of TEC modules were considered. One is the high-performance Laird Thermal 199 coupler model and the generic 127 coupler modules. Both had the same footprint (40mm x 40mm x 4mm) and the same maximum current (6A at ΔT_{MAX}). The Laird models offered a higher Q_{MAX} value (85W vs. 65W), but this performance gap was reduced significantly in the operating range used in my testing. Additionally, the generic version could be purchased for \$2.50 each, while the Laird models were 15 times the cost at \$37.50 each. Since the improved performance was somewhat limited, it was decided to proceed with the 127 couplers generic TECs.

8.3 *Fan Air Duct Configurations*

The four air duct configurations tested all used the same Comair-Rotron JQ12B4 12VDC tube axial fan. These fans provided 235 cfm airflow at zero back pressure, and the

following reduced performance with increased back pressure (black/lower “B” curve).

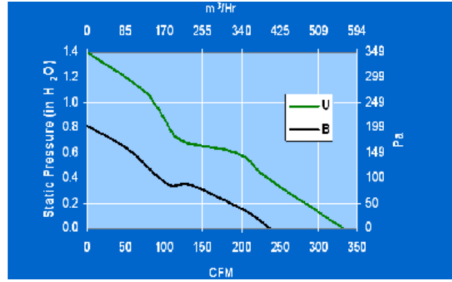


Figure 32 – Comair-Rottron Fan Performance Curve

As expected, as the flow was increasingly restricted moving from the 4-duct design down to the 1-duct design, the amount of total airflow was reduced as well. The table below indicates the volumetric flow rates for each of the four designs.

Table 8 – Volumetric Airflow Rates

Duct Design	Total Flow Rate	Individual Duct Flow Rate
4-Way Duct	72 cfm	18 cfm
3-Way Duct	66 cfm	22 cfm
2-Way Duct *	60 cfm	30 cfm
1-Way Duct *	45 cfm	45 cfm

*estimate

8.4 *TEC Grid Configurations*

To properly compare the performance of the four different TEC grid configurations, the same total current was provided to each grid of TECs. When performing the CFD analysis to determine the steady-state temperature distribution on the condensation plates, it was determined that using a bulk temperature or average surface temperature exclusively to compare the performance of each configuration was not adequate. With

the one and two TEC grids, there were every large temperature gradients across the 8-1/2" x 8-1/2" condensation plate, which did not provide a large enough area to extract water from the air. Additionally, with the concentrated low temperature near the center of the one and two TEC devices, there was a tendency for the 40°F target temperature to be exceeded on the low side which could result in a freeze-up of the water.

To determine if the simulation results were correlated with the actual test results, a FLIR C2 infrared camera was utilized to determine the temperature distribution across the four TEC grid configurations. Sample video footage of the testing can be seen at www.engr1304.com.

The three and four TEC grid pattern configurations gave the best balance between even temperature distribution and low (but not below 40°F) condensation plate temperatures. However, even with the four TEC grid configurations, a substantial temperature gradient was seen in the analysis and during the actual testing, an example of which can be seen in the following figure.



Figure 33 – Condensation Plate Temperature Distribution

8.5 *Heat Sink / Heat Pipe Configurations*

The four heat sink/heat pipe assemblies were all the same overall length (~7.90"). Each assembly started and ended with a 2.00" diameter radial finned heat sink with varying lengths.

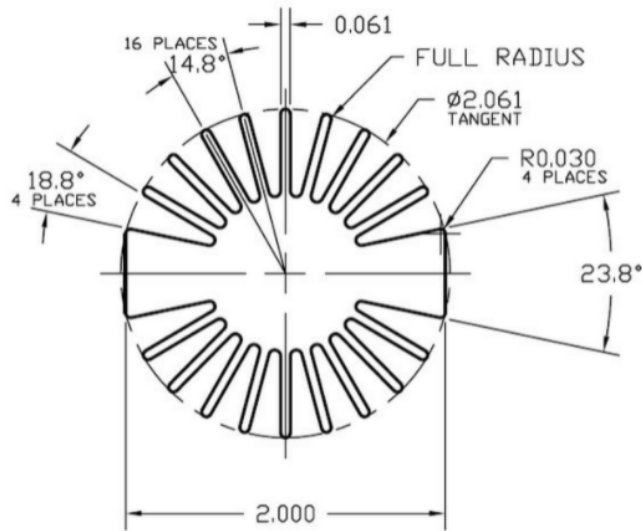


Figure 34 – Radial Aluminum Finned Heat Sink: (www.heatsinkusa.com)

In three of the four configurations, three holes were drilled in the inner ends of each pair of heat sinks. The one in the center was a 10mm hole to accommodate a 10mm 133W copper heat pipe and the two on the left and right edges were 4mm holes to accommodate a pair of 4mm 71W heat pipes. The variations on these three configurations were the portion of the stack that was heat sink and the portion that was heat pipe. The fourth configuration was all heat sink (no heat pipe).

The heat pipes are most efficient when the temperature of the evaporator (hot end) is on the high end of the operating range of the device (30°C – 120°C). Although the TEC can operate up to 100°C, in this range, the COP of the TEC is greatly reduced. Therefore, there is a conflict between trying to operate the heat pipe at its optimum temperature (~100°C) and the TEC at its optimum temperature (<40°C). To achieve a COP greater than 0.50 requires a TEC ΔT of less than 40°C, which at the 40°F (4.4°C) set point of the cold side condensation plate, would require a hot side temperature of less than 44°C, much less than the optimum temperature for the heat pipe.

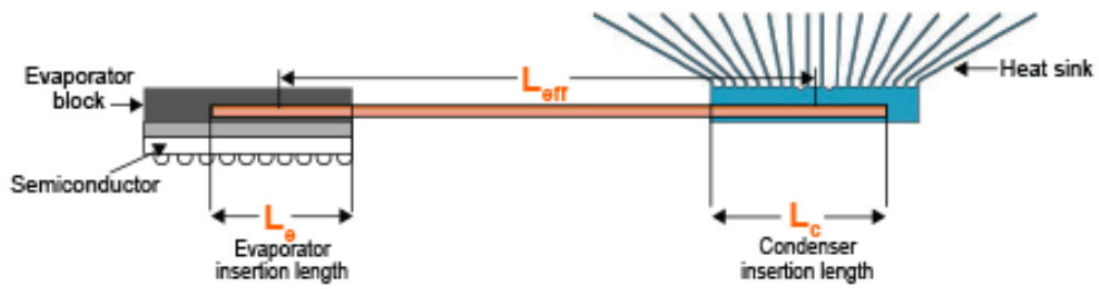


Figure 35 – Heat Pipe Design Parameters (www.heatsinkusa.com)

As confirmed with the Solidworks Flow Simulation and testing results, it was determined that there is a negligible benefit to using heat pipes in conjunction with the more traditional aluminum heat sinks.

IX. SUMMARY AND FUTURE WORK

The main challenge of the design, simulation, and testing of both the original and final AWG test platforms was trying to keep the hot side of the Peltier devices at a low enough temperature to allow them to operate at a COP value approaching 0.50. Aluminum heat sinks were used because of their high thermal conductivity, high-velocity airflow through a confined plenum system provide forced convection cooling for the heat sinks, and heat pipes were incorporated to take advantage of their superior phase transition heat transfer characteristics. Multiple grid configurations were employed to optimize a suitable combination of current/voltage settings to increase the Peltier device COP values. Two types of TEC modules (129 couple and 199 couple) versions were tested to determine the advantages of utilizing high-performance TECs.

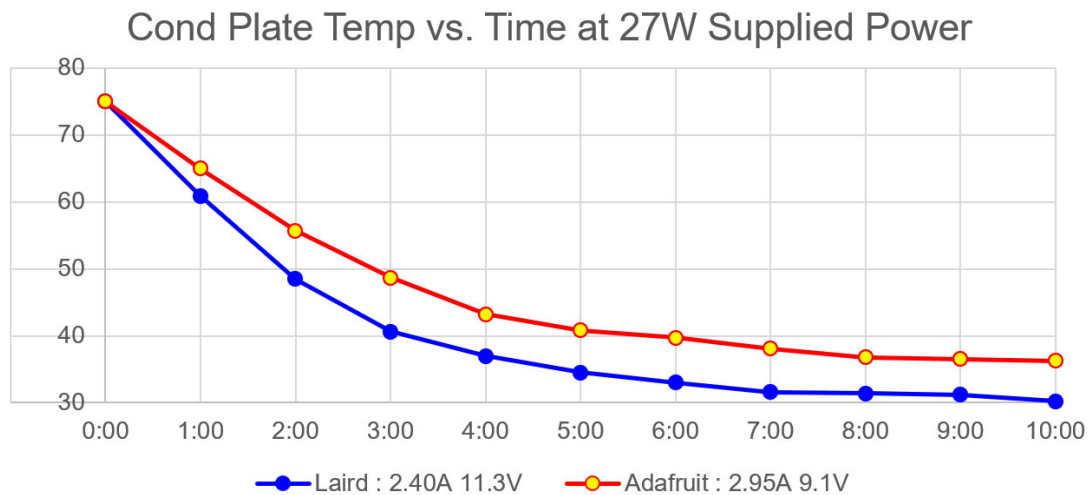


Figure 36 – 127 vs. 199 couple TEC Comparisons: Equal Power

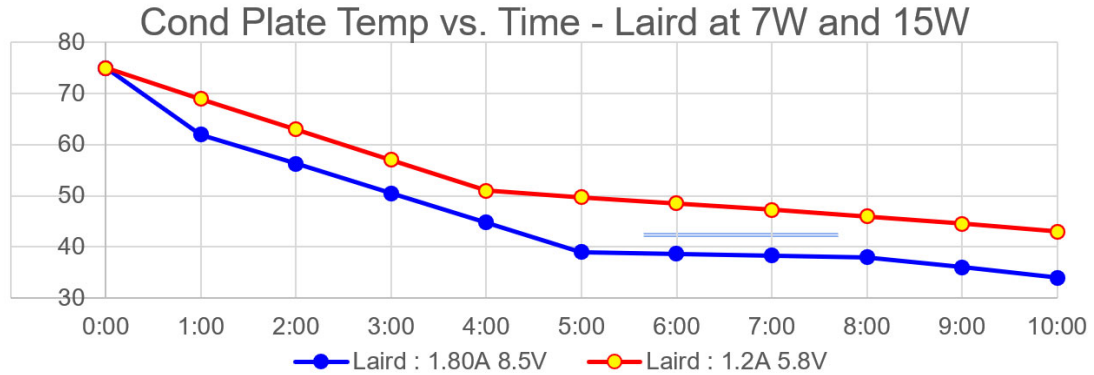


Figure 37 – Heat Pipe Design Parameters

However, regardless of how well a system is designed, the second law of thermodynamics can not be avoided. In general terms, this states that heat will flow naturally from objects of higher temperature to objects of lower temperature. Via the Peltier effect, the input DC power provided to the TEC causes heat to flow un-naturally from the cold side to the hot side. Therefore, the overall goal is to keep the hot side as cool as possible to reduce the temperature difference between the hot and cold side, thus lowering the temperature of the cold side and increasing the heat flow through the TEC, and increasing its COP.

For future work, design changes such as increasing the surface area of the heat sinks and investigating the use of surface texture geometry on the condensation plates to improve AWG.

REFERENCES

- [1] David E. Reisner, T. Pradeep, *Aquananotechnology*, CRC Press
- [2] Almusaied, Asiabanpour, A Novel Design of Hybrid Hydrophilic-Superhydrophobic Surfaces for Fog Harvesting, 2021
- [3] Davidson, K., Asiabanpour, B., & Almusaied, Z. 2017. Applying Biomimetic Principles to Thermoelectric Cooling Devices for Water Collection, 7(3), 27–35. <https://doi.org/10.5539/enrr.v7n3px>
- [4] Suryaningsih, Sri., and N.Otong. 2015. “Optimal Design of an Atmospheric Water Generator (AWG) Based on Thermo-Electric Cooler (TEC) for Drought in Rural Area.” Prepared for 2nd Padjadjaran International Physics Symposium 2015.
- [5] <https://www.bbc.com/news/world-42982959>
- [6] Esfahani, J.A., Modirkhazeni, S.M. 2012. “Modeling of Laminar, Film-Wise Condensation.” In Ahsan, Amimul, Water Condensation: Process, Modeling and Control, pp 1-70. Nova Science Publishers Inc., New York.
- [7] Wahlgren, Ronald V. 2016. “Water-from-Air Quick Guide: Second Edition”. Atmoswater Research, North Vancouver, BC.
- [8] Gao, Wei., Lv, Hao., Wang, Xiao-Dong., Yan, Wei-Mon., “Enhanced Peltier Cooling of Two-staged Thermoelectric Cooler Via Pulse Currents.” International Journal of Heat and Mass Transfer 114: 656-663.
- [9] Milani, D. & Abbas, A., Vassallo, A., Chiesa, M., & Al Bakri, D. 2011. Evaluation of Using Thermoelectric Coolers in a Dehumidification System to Generate Freshwater from Ambient Air. Chemical Engineering Science - CHEM ENG SCI. 66. 2491-2501. 10.1016/j.ces.2011.02.018.
- [10] “Steinhart & Hart Equations for 10k Thermistors” Water & Air, <http://www.skyeinstruments.com/wp-content/uploads/Steinhart-Hart-Eqn-for-10k-Thermistors.pdf>
- [11] Postel, Sandra L. “Entering an Era of Water Scarcity: The Challenges Ahead.” Ecological Applications, vol. 10, no. 4, 2000, pp. 941–948. JSTOR, JSTOR, www.jstor.org/stable/2641009

- [12] Weil, Sydney. "How Does Water Use in the United States Compare to That in Africa?" African Wildlife Foundation, 6 Sept. 2013, www.awf.org/blog/how-does-water-use-united-states-compare-africa.
- [13] Wilson, Lynn. "The Costs of Fresh Water in a Changing World (Op-Ed)." LiveScience, Purch, 22 Apr. 2014, www.livescience.com/45049-costs-of-fresh-water.html.
- [14] "Ensuring the Resiliency of Our Future Water and Energy Systems." Department of Energy, 2014, www.energy.gov/articles/ensuring-resiliency-our-future-water-and-energy-systems.
- [15] Adeoye, O.O., et al. "Atmospheric Water Generation: A Path to Net-Zero." 2016 IEEE Green Technologies Conference (GreenTech), 2016, doi:10.1109/greentech.2016.16.
- [16] "Atmospheric Water Generator Market - US\$8 Billion revenue by 2024." PR Newswire, 15 Nov. 2017.
- [17] Esfahani, J.A., Modirkhazeni, S.M. 2012. "Modeling of Laminar, Film-Wise Condensation." In Ahsan, Amimul, Water Condensation: Process, Modeling and Control, pp 1-70. Nova Science Publishers Inc., New York.
- [18] Almusaiid, Z., Asiabanpour, B. Atmospheric Water Generation: Technologies and Influential Factors." Institute of Industrial and Systems Engineers Research Conference 2017, PA, 2017.
- [19] Pontious, K., Weidner, B. Guerin, N. Dates, A. Pierrakos, O., and Altaii, K., "Design of an atmospheric water generator: Harvesting water out of thin air," 2016 IEEE Systems and Information Engineering Design Symposium (SIEDS), Charlottesville, VA, 2016, pp. 6-11. doi: 10.1109/SIEDS.2016.7489327
- [20] Wahlgren, Ronald V. 2016. "Water-from-Air Quick Guide: Second Edition". Atmoswater Research, North Vancouver, BC.
- [21] Asiabanpour, B., Ownby, N., Summers, M., Moghimi, F. (2019), "Atmospheric water generation and energy consumption: an empirical analysis", IEEE Texas power and energy conference (TPEC), 1-6

[22] Moghimi, F., Ghoddusi, H., Asiabanpour, B., Behroozikhah, M. (2019), "Atmospheric water generation (awg): performance model and economic analysis", IFIP International Conference on Advances in Production Management Systems

[23] Moghimi, F., Ghoddusi, H., Asiabanpour, B., Behroozikhah, M. (2021), "Is atmospheric water generation an economically viable solution?", Clean Technologies and Environmental Policy, 1-18.

https://www.solidworks.com/sw/docs/Flow_Basis_of_CAD_Embedded_CFD_Whitepaper.pdf